THE FASEB JOURNAL • RESEARCH • www.fasebj.org

Delivery of a TNF-α–derived peptide by nanoparticles enhances its antitumor activity by inducing cell-cycle arrest and caspase-dependent apoptosis

Qiuxia Yan,*,† Xueming Chen,* Huizhen Gong,* Pei Qiu,* Xing Xiao,* Shiying Dang,* An Hong,* and Yi Ma*,[1]

*Department of Cellular Biology, National Engineering Research Center of Genetic Medicine, Key Laboratory of Bioengineering Medicine of Guangdong Province, Institute of Biomedicine, Jinan University, Guangzhou, China; and †Center for Reproductive Medicine, The Sixth Affiliated Hospital of Guangzhou Medical University, Qingyuan People's Hospital, Qingyuan, China

ABSTRACT: Prostate cancer is the second-most common malignancy of the male genitourinary system. TNF-α has attracted intense attention as a potential therapeutic agent against various cancers. However, its therapeutic application is restricted by short half life and severe toxic side-effects. In this study, we constructed a stable nanodrug, called TNF-α–derived polypeptide (P16)-conjugated, chitosan (CTS)-modified selenium nanoparticle (SC; SCP), which is composed of SC as a slow-release carrier conjugated to the TNF-α–derived peptide P16. SCP had significant inhibitory effects on multiple types of tumor cells, especially DU145 prostate cancer cells, but not on RWPE-1 normal human prostate epithelial cells. SCP could induce G0/G1 cell-cycle arrest and apoptosis in DU145 cells more effectively than could P16 and TNF-α. In DU145 xenograft tumor models, SCP exerted much stronger antitumor effects than P16 or estramustine (the clinical drug for prostate cancer) but caused fewer toxic side-effects. In addition, SCP significantly inhibited proliferation and accelerated apoptosis in DU145 xenograft tumors. Further mechanistic studies revealed that SCP exerted antitumor effects *via* activation of the p38 MAPK/JNK pathway, thus inducing G0/G1 cell-cycle arrest and caspase-dependent apoptosis. These findings suggest that SCP may represent a potential long-lasting therapeutic agent for human prostate cancer with fewer side effects.—Yan, Q., Chen, X., Gong, H., Qiu, P., Xiao, X., Dang, S., Hong, A., Ma, Y. Delivery of a TNF-α–derived peptide by nanoparticles enhances its antitumor activity by inducing cell-cycle arrest and caspase-dependent apoptosis. FASEB J. 32, 000–000 (2018). www.fasebj.org

KEY WORDS: P16 · nanoselenium · slow-release carrier · prostate cancer

Prostate cancer is the second-most commonly diagnosed malignancy among males worldwide, and 1.1 million new cases are estimated to have occurred in 2012 (1). Recently, the incidence of prostate cancer has rapidly increased in China and seriously impacts the health of Chinese men. Prostate cancer has been deemed to be an ideal tumor type for chemoprevention because of its extended latent stage, increased incidence with age, and multistep signaling pathway mechanism (2, 3). Unfortunately, most of the traditional cancer drugs for prostate cancer are far from satisfactory, as they possess a comparatively short half life ($t_{1/2}$), poor permeability, and a broad range of side-effects. Hence, it is urgent to develop novel chemotherapeutic drugs for prostate cancer treatment (4).

TNF-α, which is a critical cytokine, mainly produced by macrophages, is one of the most promising agents for cancer treatment (5, 6). TNF-α plays many important roles in physiologic and pathologic events; for instance, it can cause tumor cell necrosis (including cell swelling, organelle destruction, and ultimately, cell lysis) and apoptosis (including cell atrophy, chromatin condensation, and DNA fragmentation). The TNF-α genes are located on chromosome 7 and chromosome 6 in mice and humans, respectively (7). Both genes include 4 exons and are ~3 kb in size. The TNF-α genes are present in a single copy. Human TNF-α contains 157 aa residues and a propeptide of 76 aa residues. The 2 cysteine residues at positions 69 and 101 of mature TNF-α, which form the intramolecular

ABBREVIATIONS: ALB, albumin; ALT, alanine transaminase; AST, aspartate transaminase; AUC, area under the curve; BUN, blood urea nitrogen; CDK, cyclin-dependent kinase; CK, blank control; CKI, cyclin-dependent kinase inhibitor; CL, clearance; CREA, creatinine; CTS, chitosan; DBILI, direct bilirubin; EDX, energy-dispersive X-ray; EE, encapsulation efficiency; Est, estramustine; FTIR, Fourier transform infrared spectroscopy; GLB, globin; H398, a TNF receptor 1-selective inhibitor; IBILI, indirect bilirubin; IC_{50}, half-inhibitory concentration; Id2, DNA-binding 2; LE, drug loading efficiency; MTT, 3-(4,5-dimethylthiazol-2-*yl*)-2,5-diphenyltetrazolium bromide; NP, nanoparticle; P16, TNF-α–derived polypeptide; PI, propidium iodide; rmhTNF-α, recombinant TNF-α mutant; SC, chitosan-modified selenium nanoparticle; SCP, TNF-α–derived polypeptide-conjugated, chitosan-modified selenium nanoparticle; SEM, scanning electron microscopy; SeNP, selenium nanoparticle; $t_{1/2}$, half life; TBILI, total bilirubin; TEM, transmission electron microscopy; TNFR, TNF-α receptor

[1] Correspondence: Department of Cellular Biology, National Engineering Research Center of Genetic Medicine, Key Laboratory of Bioengineering Medicine of Guangdong Province, Institute of Biomedicine, Jinan University, 601 Huangpu Ave. West, Guangzhou 510632, China. E-mail: tmayi@jnu.edu.cn

doi: 10.1096/fj.201800377R

disulfide bond, are important in maintaining the tertiary structure of TNF-α (8). The bioactivities of TNF-α rely on its binding to 2 specific receptors, namely TNF-α receptor (TNFR)1 and TNFR2, on the cell membrane (9). TNFR1 contains an intracellular death domain capable of triggering apoptosis, whereas TNFR2 lacks the death domain and is related to cell proliferation (10, 11). Since the 1960s, genetically engineered TNF-α products have been used in the clinical cancer therapy. However, TNF-α is able to activate both TNFR1 and TNFR2, and TNFR2-mediated cell proliferation can neutralized the cell death *via* TNFR1 activation (12). More unfortunately, as an immune stimulator and endogenous pyrogen, TNF-α produces intolerable side-effects, such as septic shock, cachexia, and fever, and it has a short $t_{1/2}$ (15–30 min) and poor bioavailability (13). Thus, TNF-α derivatives, such as TNFR1-specifc agonists, may effectively aggravate tumor destruction without causing side-effects and will be proposed as potential prostate cancer therapeutics.

Small molecular polypeptides have been a new focus in the production of antitumor drugs, owning to their favorable characteristics, such as a lack of immunogenicity, potent bioactivity, and excellent penetration to cancer cells (14). Therefore, polypeptides derived from TNF-α may possess ameliorated antitumor efficacy. One of the active sites of TNF-α is the region of amino acid residues 84–91 (15). In addition, our previous studies demonstrated that TNF-α–derived polypeptide (P16), which is composed of amino acid residues 75–94 (LLTHTISRIAVSYQTKVNLL) of TNF-α, could selectively bind to TNFR1 and that it exhibited good antitumor efficacy. However, P16 has a comparatively low MW of 2.27 kDa and possesses a very short $t_{1/2}$ (~5.77 min) and poor bioavailability, owning to its rapid renal clearance (CL) and hepatic metabolism (16). Therefore, the development of new drug delivery carriers for cancer treatment is urgently needed to overcome these disadvantages.

Nanomaterials are currently used extensively as drug carriers for cancer treatment (17, 18). Thus far, a variety of nanomaterials with different functions, such as polymers, mesoporous silica, and carbon nanotubes, have been developed for cancer treatment (19–21). Among these nanomaterials, selenium nanoparticles (SeNPs) are attracting increasing attention as potential drug nanocarriers because of their lower toxicity, more robust biologic activities, and higher bioavailability than organic or inorganic selenocompounds (22, 23). In addition, chitosan (CTS), which is an α (1–4)-linked 2-amino-2-deoxy-β-D-glucose unit, can undergo specific chemical modifications to produce a wide range of derivatives, as it has the principal amidogen in the C-2 position and the hydroxyl in the C-6 position of its monomeric units. CTS is one of the most extensively used biopolymers for nanoparticle (NP) preparation as a result of its biodegradability, biocompatibility, pH sensitivity, low immunogenicity, and low toxicity. Because of these beneficial properties, CTS-modified NPs are emerging as one of the most promising delivery carriers for cancer chemotherapy (24).

To overcome the limitations of the therapeutic efficacy of P16, in the present study, we constructed stabilized CTS-modified SeNPs (termed SC) as a slow-release carrier to combine the TNF-α–derived peptide P16 through the formation of an amide bond between the amino group of SC and the tyrosine carboxyl group of P16. First, the morphology, size, ζ potential, elemental composition, drug loading efficiency (LE), and release behavior of P16-conjugated, CTS-modified SeNP (SCP) *in vitro* were evaluated by various biochemical methods. Next, we examined whether SCP exhibits selectivity between cancer cells and normal cells, and we measured the difference in the inhibition of SCP, SC, and free P16 by 3-(4,5-dimethylthiazol-2-*yl*)-2,5-diphenyltetrazolium bromide (MTT) assays. Then, we investigated changes in apoptosis and in the cell cycle in DU145 cells in response to treatment with SCP to elucidate its antitumor effect. Finally, we examined the antitumor mechanism of SCP in mouse DU145 xenograft tumor models and speculated that SCP inhibited tumor growth through activating the p38 MAPK/JNK signaling pathway, thus inducing G_0/G_1 cell-cycle arrest and the caspase-dependent apoptosis.

MATERIALS AND METHODS

Materials

Peptides P16 were synthetized by Sinoasis Pharmaceutical Factory (Guangzhou, China). Sodium selenite (Na_2SeO_3), thiazolyl blue tetrazolium bromide (MTT), and DAPI were obtained from MilliporeSigma (Burlington, MA, USA). An Annexin V-FITC/propidium iodide (PI) kit and PI were purchased from TransGen Biotech (Beijing, China). A TUNEL assay kit was purchased from Roche (Basel, Switzerland). Fetal bovine serum and Roswell Park Memorial Institute-1640 medium were purchased from Thermo Fisher Scientific (Waltham, MA, USA). TNF-α and estramustine (Est) were obtained from Phamacia (Stockholm, Sweden). An inhibitor of TNFR1 (H398) was purchased from Abcam, Inc. (Cambridge, United Kingdom). DU145 prostate cancer cells, PC3 prostate cancer cells, LnCAP prostate cancer cells, MCF-7 breast cancer cells, MDA-MB-231 breast cancer cells, Eca109 esophageal cancer cells, HeLa cervical cancer cells, K562 leukemia cells, Raji lymphoma cells, RWPE-1 normal human prostate epithelial cells, and MCF10A nontumorigenic human mammary epithelial cells were purchased from Shanghai Institute of Cell Biology, Chinese Academy of Sciences (Shanghai, China). Ascorbic acid (vitamin C) was purchased from Guangzhou Chemical Reagent Factory (Guangzhou, China). All of the antibodies used in this research were purchased from Cell Signaling Technology (Danvers, MA, USA) with the exception of Cy3-conjugated goat anti-rabbit IgG (from Servicebio, Wuhan, China). The water used in all experiments was ultrapure water produced by the Milli-Q water purification system (MilliporeSigma).

Preparation of peptide SCP

SCP was synthesized as follows: in brief, 100 μl of 0.8 mg/ml CTS was gradually added into 1 ml of 5 mM sodium selenite (Na_2SeO_3) under magnetic stirring, and 1 ml of 20 mM ascorbic acid solution (vitamin C) was then added into the mixture. After the mixture was allowed to incubate for 30 min at 4°C, it was dialyzed overnight at 4°C; the SC was then obtained. A stock solution of 2 mg/ml P16 was prepared by dissolving 2 mg P16 powder in 1 ml PBS, and this solution was then mixed with the previously prepared SC solution. After the final volume of the solution was adjusted to 5 ml with Milli-Q water, the coupling reaction was performed using 1-ethyl-3-(3-dimethylaminopropyl) carbodiimide hydrochloride and *N*-hydroxysuccinimide as the active catalysts, with magnetic stirring at room temperature for

12 h. Finally, the solution was dialyzed overnight at 4°C, and the peptide SCP was then prepared (**Fig. 1**).

Morphology and characterization of SCP

Various kinds of approaches were used to characterize the properties of the prepared NPs. The morphology of SC and SCP was visualized by transmission electron microscopy (TEM) and scanning electron microscopy (SEM) after the samples were freeze dried. To characterize the size distribution and ζ potential of these NPs, a Zetasizer Nano analyzer (Malvern Instruments, Manchester, United Kingdom) was used. The absorption peak of SCP in a wavelength's range of 400–4000 cm^{-1} was detected by Fourier transform infrared spectroscopy (FTIR). The elemental composition of SCP was analyzed by energy-dispersive X-ray (EDX) spectrometry. The stability of SCP was continuously monitored for 40 d using the Zetasizer Nano analyzer, and the changes in size distribution were used to evaluate the stability.

In vitro determination of encapsulation efficiency, LE, and drug-release assay

The amount of free P16 was assessed by the HPLC technique. In brief, 100 μl SCP solution was placed in a 1-ml, 10 kDa Ultrafiltration Tube (MilliporeSigma) and centrifuged at 4000 rpm for 30 min before dialysis. The filtrate was collected, and the quality of the peptide P16 was measured using HPLC. The P16 encapsulation efficiency (EE) and drug LE were calculated using the following formulas:

$$\mathrm{EE} = \frac{\text{total P16 mass} - \text{mass of free P16}}{\text{total P16 mass}} \times 100\%$$

and

$$\mathrm{LE} = \frac{\text{total P16 mass} - \text{mass of free P16}}{\text{SCP mass}} \times 100\%$$

The *in vitro* drug-release assay analyzing the release of P16 from SCP was performed using a dialysis method as reported previously (25). In brief, 60 μg SCP powder was dissolved in 1 ml PBS (pH 7.5) and packed into a dialysis tube. The tube was then immersed in 60 ml PBS under constant shaking at 200 rpm at room temperature. At scheduled time intervals (0, 4, 8, 12, 16, 20, 24, 28, 32, 36, 40, and 44 h), a 1-ml sample of the PBS outside of the dialysis tube was removed and was replaced with an equal volume of fresh PBS. The amounts of drug released into the PBS outside the tube were detected by HPLC.

Effects of SCP on proliferation in multiple cancer cell lines and in 2 normal epithelial cell lines

Cell viability was determined by measuring the ability of cells to transform MTT to purple formazan crystals (26). In this study, we investigated the effect of SCP on cell viability in 9 human cancer cell lines (the DU145, PC3, and LnCAP prostate cancer cell lines; the MCF-7 and MDA-MB-231 breast cancer cell lines; the Eca109 esophageal cancer cell line; the HeLa cervical cancer cell line; the K562 leukemia cell line; and the Raji lymphoma cell line) and 2 normal epithelial cell lines (the RWPE-1 normal human prostate epithelial cell line and the MCF10A nontumorigenic human mammary epithelial cell line). In brief, cells in the logarithmic growth phase were seeded in 96-well plates at a density of 1×10^4 cells/well and allowed to adhere in complete medium at 37°C for 24 h. The cells were then incubated with SCP at different concentrations for 48 h. Then, the old culture medium was discarded, and the cells were washed twice with PBS. Subsequently, 20 μl MTT solution (5 mg/ml in PBS) was added to each well, and incubation was continued at 37°C for an additional 4 h. Formazan crystals, formed by living cells, were dissolved in 150 μl/well DMSO. The color density of the formazan solution, which reflects the cell viability, was detected at a wavelength of 570 nm using a Model 680 microplate reader (Bio-Rad, Berkeley, CA, USA). The half-inhibitory concentration (IC_{50}) was determined as the concentration at which a 50% loss of viability, relative to that of untreated cells, occurred. For each cell line, the experiment was performed 3 times. In addition, we investigated the inhibitory effect of SC and SCP on the proliferation of DU145 cells by treating the cells with a series of equivalent doses of SC or SCP (0, 2, 5, 10, 20, 40, and 80 μM). Furthermore, the inhibitory effect of P16, SCP (20 μM, at the equivalent dose of P16), TNF-α, and

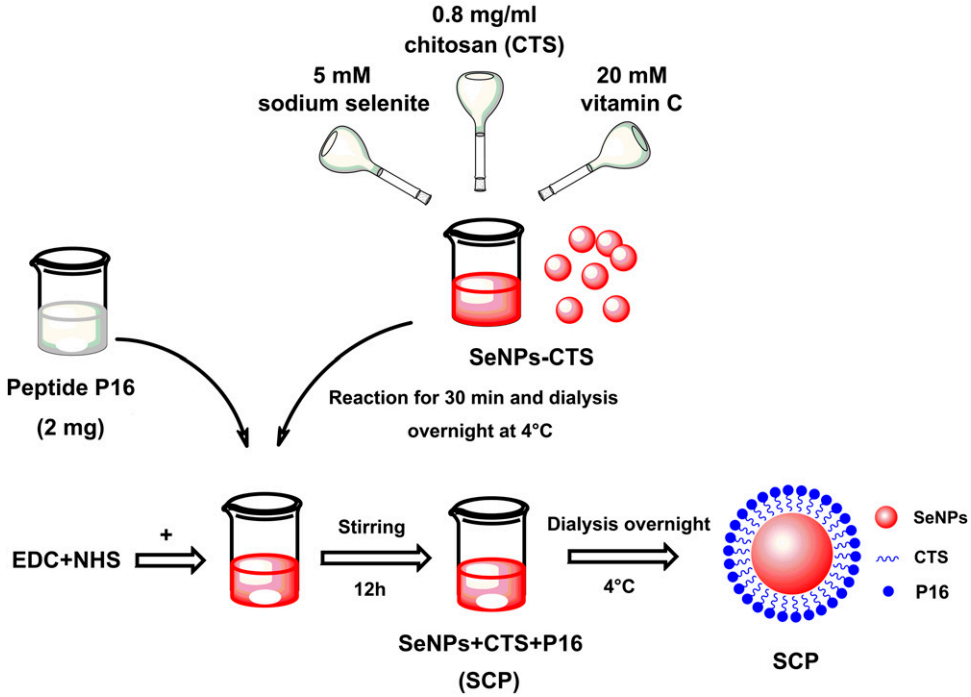

Figure 1. Schematic illustration of the steps in the preparation of SCP. SCP is composed of a spherical SeNP core coated with P16 through attachment to CTS. EDC, 1-ethyl-3-(3-dimethylaminopropyl) carbodiimide hydrochloride; NHS, *N*-hydroxysuccinimide.

SCP + H398 on the proliferation of DU145 cells was assessed by MTT assays. SeNPs and SC (at the equivalent dose of SeNPs) were used to ascertain any potential toxic effect on DU145 cells. The MTT procedure was the same as that described above.

Cell cycle analysis and the apoptosis assay *in vitro*

To analyze the cell-cycle distribution, DU145 cells were incubated in the culture medium containing 20 μM SCP (at the equivalent dose of P16) for 24 h at 37°C in 5% CO_2 and were harvested by centrifugation. The harvested cells were washed with cold PBS and fixed with precooled 70% ethanol overnight at 4°C. Then, the fixed cells were washed with cold PBS again and stained with 20 μg/ml PI in the dark for 30 min at 37°C. A DNA histogram of the cell population in the G0/G1, S, and G2/M phases was generated by flow cytometry with CellQuest software (BD Biosciences, San Jose, CA, USA).

Apoptosis rates of DU145 cells were evaluated using an Annexin V-FITC/PI staining kit. In brief, cells were seeded at a density of 2×10^5 cells/well in 12-well plates and were incubated for 24 h. The medium was refreshed with new medium containing PBS, SC, P16, SCP, TNF-α, or SCP + H398, and the cells were then cultured for 24 h. After treatment, the cells were washed twice with cold PBS and harvested by centrifugation. The cells were resuspended in 100 μl binding buffer, stained with 5 μl Annexin V-FITC and 5 μl PI, and incubated in the dark for 15 min at room temperature. Before detection, binding buffer was added to the cells to a total volume of 500 μl. Finally, the apoptotic proportion of the treated cells was measured using a flow cytometer (BD Biosciences). For each experiment, 10,000 events per sample were recorded.

Animals and treatment

Thirty-three male 4-wk-old BALB/c (25–30 g) and 30 male 4-wk-old BALB/c-nu/nu nude mice (18–20 g) were purchased from the Beijing Huafukang Bioscience (Beijing, China). All research and procedures involving mice were approved by the Animal Care Committee of Jinan University. The mice were housed in cages under specific pathogen-free conditions with a 12-h light/dark cycle at least 7 d before the experiments were performed. The ambient conditions were strictly controlled at a constant temperature of 21–23°C and a relative humidity of 40–60%. The mice were fed with standard rodent chow and distilled water *ad libitum*.

A pharmacokinetic assay was used to study the potency of SCP in blood circulation. In brief, BALB/c mice were randomly divided into 3 groups (n = 11). One group was administered TNF-α at a dose of 5 mg/kg as a positive control, and the other 2 groups were administered concentrations of SCP and P16 in accordance with the concentration of TNF-α. Compounds were delivered through the tail-vein injection. Orbital blood samples were collected from 3 mice at different time points (0, 0.25, 0.5, 1, 2, 4, 8, 12, 16, 24, and 48 h), and the concentrations of SCP, P16, and TNF-α were analyzed using the liquid chromatography/mass spectrometry method (27). Thereafter, the data for the relevant pharmacokinetic parameters were analyzed and fitted to a 2-compartment elimination model. The area under the blood concentration curve (AUC), the $t_{1/2}$ of the medicine, and the plasma CL were calculated by WinNonlin v.5.1 software (Pharsight Inc., Mountain View, CA, USA).

The *in vivo* antitumor efficacy of SCP was analyzed in mouse DU145 xenograft tumor models. After acclimatization, BALB/c-nu/nu nude mice were weighed and randomly assigned into 6 groups (n = 5). The nude mice in each of the 5 experimental groups were subcutaneously injected into the right rear flank with 0.1 ml of a DU145 cell suspension (1.0×10^7 cells/ml). The mice in the remaining group were not inoculated with DU145 cells. One week after inoculation, the mice in each experimental group were injected with 0.9% NaCl (negative control group), SCP, P16, TNF-α, or Est (positive control group) through the tail vein in a volume of 0.1 ml (once a day for 30 consecutive days). The day that the mice were treated with the drugs was designated d 1. Tumor volumes were measured every 3 d during the treatment using calipers, and tumor growth curves for each group were plotted. The tumor growth inhibition rates were calculated using the following formula: inhibition rate (%) = 1 − (average tumor weight of test group/average tumor weight of control group) × 100%. Tumor volumes were calculated by measuring the lengths and widths of the tumors. To evaluate possible toxic effects of the therapy, the body weight of each mouse was also measured during the period of the experiment. The mice that were not inoculated with DU145 cells were used as the blank control (CK) group.

One month after administration, the mice were euthanized, and the tumors were collected and weighted. The blood samples were collected for hematologic examination by quickly extracting the eyeball at the First Affiliated Hospital of Jinan University. The blood biochemical indexes aspartate transaminase (AST), alanine transaminase (ALT), albumin (ALB), globin (GLB), ALB/GLB, blood urea nitrogen (BUN), creatinine (CREA), total bilirubin (TBILI), direct bilirubin (DBILI), and indirect bilirubin (IBILI), which are closely associated with liver/kidney function, were determined by biochemical instrumentation.

Ki67 immunofluorescence assay

Ki67 is an immunohistochemical proliferation marker in many types of cancer. All mice were euthanized at the end of the trial. Tumor tissues were collected, fixed in 4% paraformaldehyde for >24 h, and embedded in paraffin. The paraffin-embedded tumors were cut into 4 mm sections. Sections were deparaffinized by melting, followed by rehydration, and were incubated in citric acid antigen repair buffer for 10 min in a steamer. After being blocked with 3% bovine serum ALB, sections were incubated with a Ki67 antibody overnight at 4°C. The next day, sections were rinsed 3 times with PBS and were then subsequently incubated with Cy3-conjugated goat anti-rabbit IgG for 1 h at room temperature. Finally, sections were counterstained with DAPI for 15 min at room temperature. After 3 washes with PBS, sections were mounted onto coverslips with antifade mounting medium and examined under a fluorescence microscope (Nikon Eclipse C1). The positive cells were quantified by analyzing the percentage of stained cells in the tumor relative to the total cell number.

TUNEL assay

DNA fragmentation was examined with fluorescence staining by a TUNEL apoptosis detection kit, according to the manufacturer's instructions. In brief, tumor sections on slides were deparaffinized and rehydrated before proteinase K was added for antigen retrieval. After permeabilization with 0.1% Triton X-100 in PBS, the sections were incubated with a TUNEL reaction mixture containing terminal deoxynucleotidyl transferase and a nucleotide mixture for 2 h and were counterstained with DAPI for 15 min at room temperature. After 3 washes with PBS, sections were mounted onto coverslips with antifade mounting medium and examined under a fluorescence microscope. The positive cells were also quantified by analyzing the percentage of stained cells in the tumor relative to the total cell number.

Western blotting

To explore the expression levels of proteins that are related to various signaling pathways in tumor tissue under treatment by

different drugs, Western blotting was performed as follows. At the termination of the experiment, all mice were euthanized, and the tumors from the different groups were excised and lysed with RIPA lysis buffer (Beyotime Institute of Biotechnology, Haimen, China) in the presence of PMSF for 1 h on ice. After the protein concentration in the cytosolic extract was determined by a Bicinchoninic Protein Assay Kit (Thermo Fisher Scientific), equal amounts of the proteins (~30 μg) were separated by 12% SDS-PAGE and were transferred onto PVDF membranes. After being blocked with 5% bovine serum ALB for 1 h at room temperature, membranes were hybridized overnight at 4°C with different primary antibodies, respectively. The next day, the membranes were washed 3 times with Tris-buffered saline containing 0.1% Tween-20 for 10 min each time. Thereafter, membranes were incubated for an additional 1 h at room temperature with appropriate horseradish peroxide-conjugated second antibodies. Protein bands were detected using West Pico Chemiluminescent Substrate (Thermo Fisher Scientific). The gray intensity of protein band was determined by ImageJ analysis software (National Institutes of Health, Bethesda, MD, USA). To control for protein loading, membranes were stripped and were then incubated with a β-actin antibody.

Statistical analysis

All data in this study are expressed as the means ± SD. Statistical analysis was performed using Prism software (GraphPad Software, La Jolla, CA, USA) by the parametric ANOVA test as appropriate. Differences with $P < 0.05$ or $P < 0.01$ were considered statistically significant.

RESULTS

Preparation and physicochemical analyses of peptide SCP

Homogenous and stable SCP NPs were prepared by an oxidation-reduction reaction. The appearance of color in SeNPs, SC, and SCP showed obvious changes, and the color of the SeNPs was deeper than that of SCP (**Fig. 2*A***). TEM and SEM images of SC in the absence and presence of P16 are shown in Fig. 2*B–E*, respectively. SCP NPs were larger than SC NPs and maintained a homogenous and monodisperse spherical structure, suggesting that surface modifications with P16 did not change the shapes of the SC NPs.

Compared with the average size of SC NPs (72.78 nm), the average sizes of SCP NPs were dramatically increased (168.8 nm; **Fig. 3*A, B***). Following the conjugation of P16 onto the SC surface, the ζ potential of SCP dramatically increased to 35.9 mV from 29.1 mV, indicating that SCP displayed greater stability than SC and SeNPs (Fig. 3*C*). SCP NPs were further characterized by FTIR to determine the chemical binding of P16 onto the SC surface. The FTIR spectral analysis of free P16, SC, and SCP is shown in Fig. 3*D*. The strong absorption band of P16 at 1105.4 cm^{-1} was attributed to −C = O stretching of the amide bond, and the strong absorption band of SC at 1658.7 cm^{-1} was attributed to −N–H stretching vibration. The FTIR spectrum of SCP resembled the spectra of P16 and SC, thus providing clear evidence that peptide P16 had been successfully conjugated to the SC surface by the interaction of the tyrosine carboxyl group (−COOH) of P16 with the amino group (–NH) of the SC carrier surface (Fig. 3*D*). Subsequently, EDX spectroscopy indicated the percentage of atoms C (37.77%), N (10.10%), O (13.12%), and Se (39.01%) in SCP; no other element was detected, thus, further confirming the conjugation of P16 to the SC surface (Fig. 3*E*). In addition, stability tests revealed that the size of SCP and SC NPs remained stable in the aqueous solution for at least 36 d without precipitating. However, we found that the size of SCP alone dramatically increased up to ~500 nm on d 40, as the aggregation and precipitation of SeNPs were likely beginning to occur (Fig. 3*F*). Therefore, the high uniformity and stability of SCP could offer support for its application as a cancer therapeutic in the future.

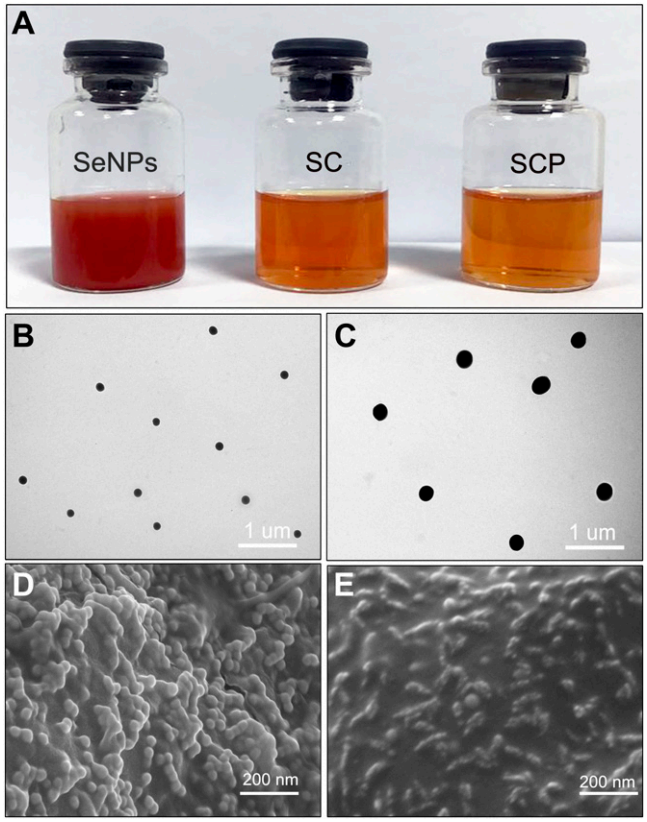

Figure 2. The morphology of SeNPs, SC, and SCP. *A*) Color of SeNPs, SC, and SCP. *B*, *C*) TEM images of SC and SCP. Original scale bars, 1 μm. *D*, *E*) SEM images of SC and SCP. Original scale bars, 200 nm.

Loading rate and drug-release studies

The EE and LE of peptide P16 onto SC were determined using HPLC, and the results showed that the EE was 71.5 ± 3.38% and that the LE was 64.98 ± 7.31%. The high loading rate of P16 onto SC, observed in this work, was similar to that observed in our previous study (28). SeNPs exhibited a narrow margin between favorable and toxic effects. As a result of the high LE of SC, the dose of SC could be decreased to minimize the potential side-effects. Moreover, a low dose of SeNPs exhibited excellent antitumor activity, which may induce tumor cells to undergo apoptosis. However, the antitumor mechanism of SeNPs needs further investigation.

To achieve prolonged systemic circulation, sustained-release NPs should be constructed. Figure 3*G* shows that

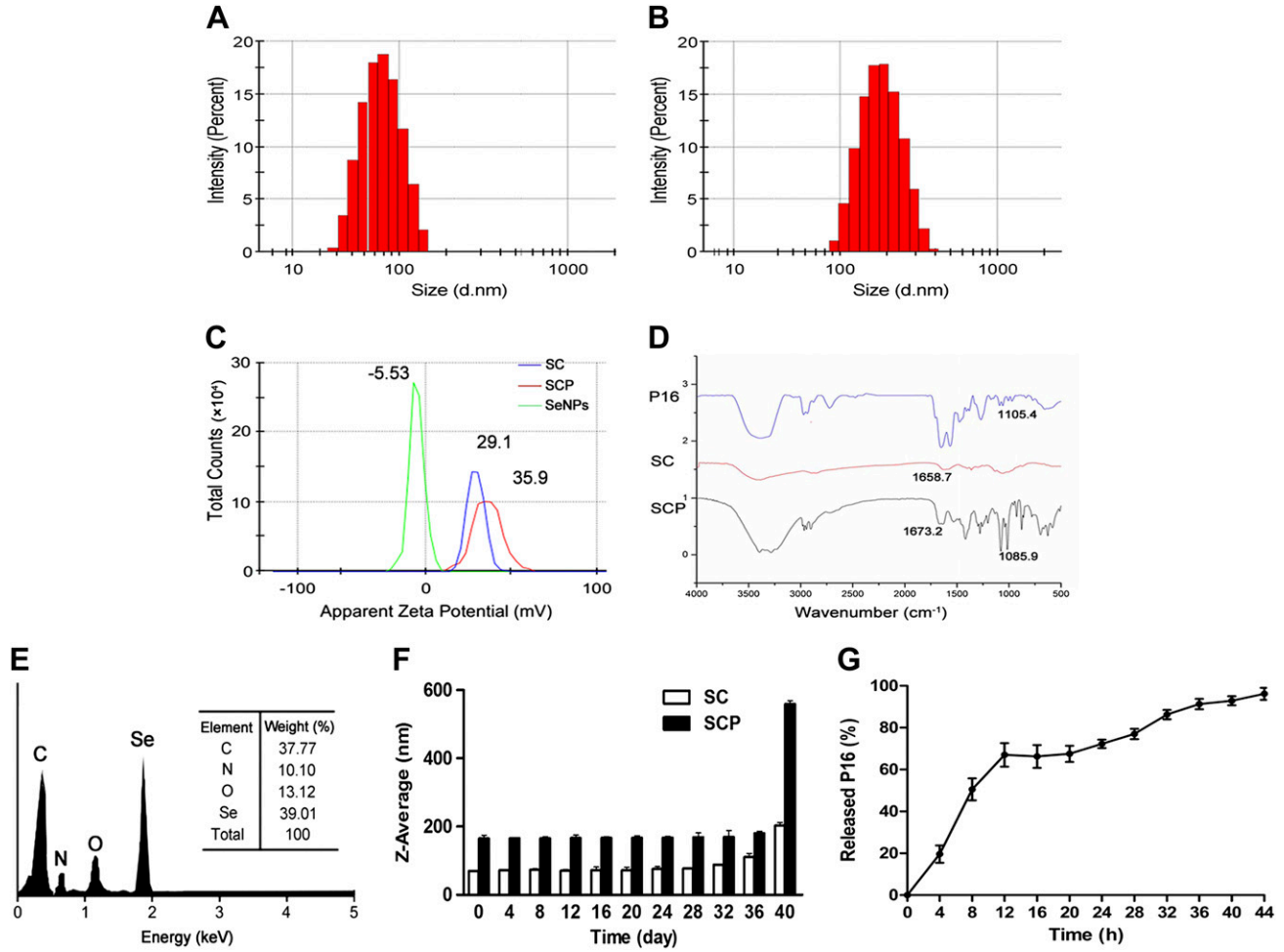

Figure 3. Characterization of SeNPs, SC, and SCP. *A*, *B*) Size distribution of SC and SCP. *C*) Zeta potential of SeNPs, SC, and SCP. *D*) FTIR of P16, SC, and SCP. *E*) EDX spectroscopy of SCP. *F*) SC and SCP maintained their original size and remained nonaggregated for an extended period of time. However, SCP was very unstable and formed large aggregates rapidly (particle size increased from ~200 to ~500 nm on d 40). *G*) The release of P16 from SCP proceeded in a controlled manner, with 67% of P16 released at 12 h and 97.94% at 44 h.

during the first 12 h, the initial release of P16 from SCP increased dramatically, up to 67%. This period was followed by one of gradual release, in which the cumulative release rate reached 97.94% after 44 h of incubation; these results exhibited a good sustained-release effect of P16 from SCP. The drug-release burst, observed during the first 12 h, was possibly attributed to the weak adsorption of the outer-layer protein, whereas the slower drug release at 13–44 h was likely a result of the stable interaction by chemical bonding and the strong electrostatic force. Because of the excellent protein-loading capacity and the slow-release pattern of SC, SC could be used as a promising, controlled release system for cancer therapy.

SCP inhibited the proliferation of multiple types of tumor cells but not the proliferation of normal human prostate epithelial cells (RWPE-1) or nontumorigenic human mammary epithelial cells (MCF 10A)

The *in vitro* inhibitory effect of SCP against various human cancer cell lines was first screened by an MTT assay. The cell lines included the DU145, PC3, and LnCAP prostate cancer cell lines; the MCF-7 and MDA-MB-231 breast cancer cell lines; the Eca109 esophageal cancer cell line; the HeLa cervical cancer cell line; the K562 leukemia cell line; and the Raji lymphoma cell line. As shown in **Fig. 4*A***, SCP exhibited a broad-spectrum inhibition against proliferation in these cancer cell lines, with different IC_{50}. Although SCP significantly inhibited the proliferation of PC3 and LnCAP cells with the IC_{50} values of 49.21 ± 5.23 and 55.09 ± 6.01 μM, respectively, the strongest inhibitory effect of SCP was observed for DU145 cells, for which the IC_{50} value was 13.10 ± 4.24 μM. Despite this potency, SCP showed lower inhibition toward RWPE-1 normal human prostate epithelial cells and MCF10A nontumorigenic human mammary epithelial cells than toward cancer cells; the IC_{50} values for RWPE-1 and MCF10A cells were 177.38 ± 12.59 and 171.69 ± 9.95 μM, respectively. Interestingly, RWPE-1 cells were used as a model to compare the effects of SCP on normal prostate cells with the effects of SCP on human prostate cancer cells. The results showed that SCP exhibited

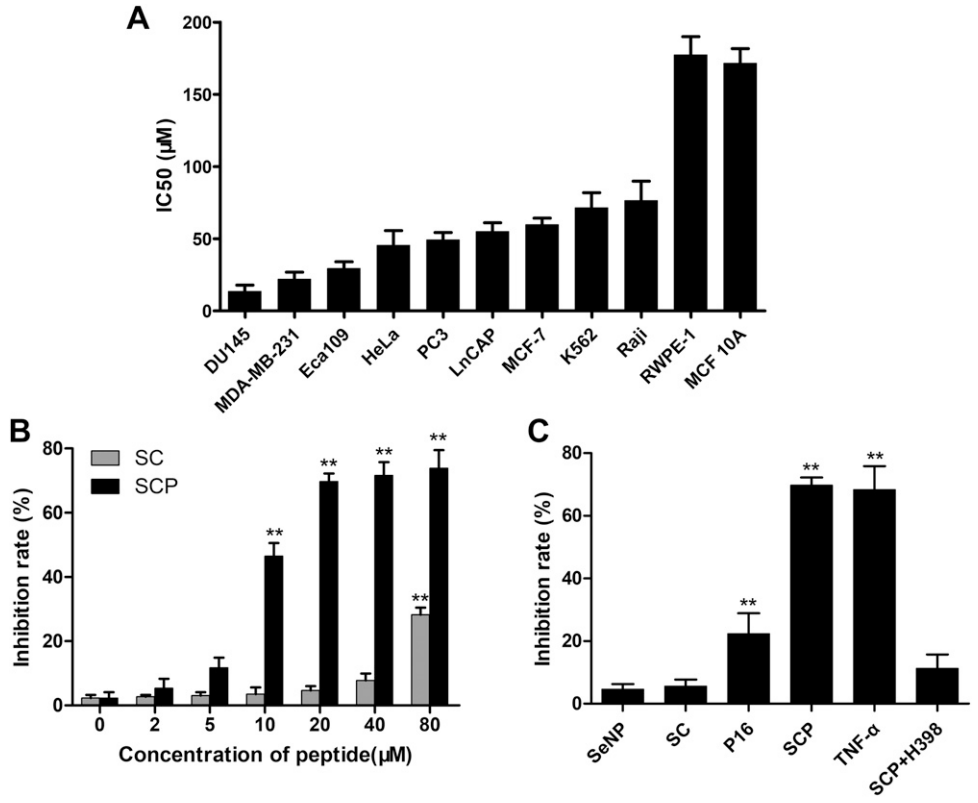

Figure 4. SCP inhibited DU145 cell proliferation, as determined by an MTT assay. *A*) SCP exhibited broad-spectrum inhibition of the proliferation against various types of cancer cells, with different IC_{50}; however, it had no significant inhibitory effect on normal human prostate epithelial cells (RWPE-1) and nontumorigenic human mammary epithelial cells (MCF 10A). *B*) SCP showed a dose-dependent inhibition of DU145 cell proliferation. $^{**}P < 0.01$, SCP *vs.* SC. *C*) The inhibitory effects of SeNP, SC, P16, SCP, TNF-α, and SCP + H398 on the proliferation of DU145 cells were detected by an MTT assay. Each experiment was repeated 3 times, and the results are expressed as the means ± SD. $^{**}P < 0.01$, SCP *vs.* SeNP or SC or P16 or SCP + H398; P16 *vs.* SeNP; TNF-α *vs.* SeNP.

lower inhibition on DU145 cells (IC_{50} = 13.10 ± 4.24 μM) than on RWPE-1 cells (IC_{50} = 177.38 ± 12.59 μM). These results suggested that the effects of SCP on the human cells are cell-type specific. This selectivity could be partially a result of the different gene expression and protein profiles of different cells, which resulted in the activation of different extracellular and intracellular signaling pathways after exposure to SCP. Therefore, DU145 cells, which had the highest susceptibility of SCP, were selected and treated with different concentrations of SCP. As shown in Fig. 4*B*, SCP exhibited an inhibitory effect on the proliferation of DU145 cells in a dose-dependent pattern. A dose of 20 μM SCP was enough to suppress the proliferation of DU145 cells by ~69.78%. However, the equivalent concentration of SC showed no inhibition on DU145 cell proliferation alone at doses lower than 80 μM, suggesting the hypotoxicity of this NP delivery system. In addition, the inhibitory effects of SeNPs, as well as those of SC, P16, and SCP, were detected in DU145 cells. SCP exhibited a significantly higher inhibitory effect than did any of the other compounds. The inhibitory effect of SCP was similar to that of TNF-α (positive control). Interestingly, pretreatment with H398 (a TNFR1-selective inhibitor) noticeably decreased the extent of cell death induced by SCP (Fig. 4*C*). Therefore, these data suggested that the TNFR1-mediated apoptosis pathway was involved in the SCP-induced death of DU145 cells. As a drug-delivery carrier, SC could markedly enhance the antitumor effect of P16 on DU145 cells. Taken together, our results suggested that SCP possesses a high degree of selectivity between cancer and normal cells and displays potential applications in cancer chemoprevention and chemotherapy.

SCP arrests DU145 cells in the G_0/G_1 phase

To illuminate the mechanism underlying the SCP-induced inhibition of proliferation, we investigated the effect of SCP on the cell-cycle distribution using flow cytometry. As shown in **Fig. 5**, the cell population in the G_0/G_1, S, and G_2/M phases was 49.16, 38.66, and 12.18%, respectively, in control DU145 cells. However, after treatment with SCP for 48 h, the G_0/G_1 population was increased to 67.51%; this increase was significantly higher than that resulting from treatment with P16 (59.84%). This increase in the G_0/G_1-phase cell population was accompanied by a concomitant decrease in the S- and G_2/M-phase cell populations. Interestingly, the cell-cycle arrest effect disappeared in DU145 cells pretreated with H398 before SCP treatment. This result suggested that SCP could inhibit the progression of cells from the G_0/G_1 phase to the S phase through a TNFR1-mediated apoptosis pathway. Although TNF-α could induce the G_0/G_1-phase arrest in DU145 cells, its inhibitory ability was weaker than that of SCP.

SCP significantly induced the apoptosis of DU145 cells

Apoptosis was one of the most important mechanisms accounting for the antitumor activity. The translocation of phosphatidylserine to the outer membrane is a significant step in the apoptosis of cancer cells (29). To quantify the cell apoptosis induced by SCP, DU145 cells were evaluated using Annexin V-FITC/PI double staining by flow cytometry. The proportion of both early apoptotic and late apoptotic cells, triggered by SCP treatment, increased to 53.5%; this increase was significantly higher than that

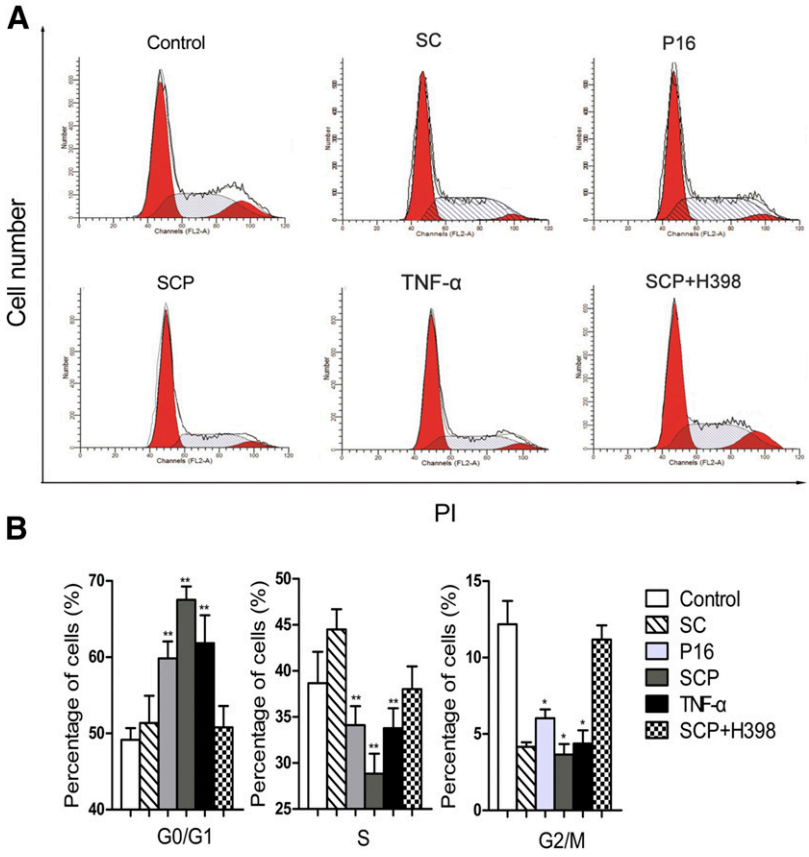

Figure 5. Cell-cycle distribution was analyzed by PI single staining by flow cytometry. *A*) Flow cytometry assays of the cell cycle for control (PBS)-, SC-, P16-, SCP-, TNF-α-, and SCP + H398-treated DU145 cells. *B*) Statistics and data analysis of the cell-cycle distribution of DU145 cells. Each value represents the mean ± SD of 3 separate experiments. $^{**}P < 0.01$, SCP or P16 or TNF-α *vs.* control or SC or SCP + H398; $^{*}P < 0.01$, SCP or P16 or TNF-α *vs.* control or SCP + H398.

triggered by P16 (15.94%). The enhanced apoptotic effect was most likely because of the enhanced cellular accumulation of P16 through SC-mediated endocytosis events. Although TNF-α could also induce DU145 cells to undergo apoptosis, its proapoptotic ability was weaker than that of SCP (**Fig. 6**). A result similar to that of the cell-cycle assay was also found; the cell proapoptotic effect disappeared in DU145 cells pretreated with 100 nM H398 before 20 μM SCP treatment. The results suggested that SCP induced the apoptosis of DU145 cells, mainly through a TNFR1-mediated apoptosis pathway. Taken together, these results indicate that SCP exerts a greater ability to arrest the cell cycle and induce the apoptosis of DU145 cells than does SC or P16, respectively. Our findings supported the feasibility of SC as a nanocarrier to enhance the antitumor effect of free P16.

The morphologic changes in the apoptotic nuclei of DU145 cells were further determined using a DAPI-staining technique. Cells were incubated with SCP, SC, P16, or TNF-α for 48 h and were then stained with DAPI for examination of the apoptotic characteristics with fluorescence microscopy. The nuclei of the control cells maintained the same size and shape, whereas the nuclei of DU145 cells, treated with SCP and TNF-α, had more chromatin condensation and nuclear condensation (an apoptotic phenotype). Similar to the results of the previous assays, when DU145 cells were pretreated with H398, the proapoptotic effect of SCP disappeared (**Fig. 7**). Collectively, these results indicated that SCP exerted the antitumor activity on DU145 cells, primarily through suppressing the cell proliferation, arresting the cell-cycle progression, and promoting the cell apoptosis.

Pharmacokinetic parameters of SCP in normal BALB/c mice

BALB/c mice, receiving a single intravenous injection of SCP, were used to investigate the pharmacokinetic parameters of SCP *in vivo*. TNF-α was used as the positive control. As shown in **Table 1**, the AUC for SCP was significantly higher than that for P16 and TNF-α. In addition, SCP displayed a notably longer circulation $t_{1/2}$ (13.52 h) than did P16 (4.2 min) and TNF-α (25.8 min). Moreover, the CL rate of SCP was 0.091 ml/h, which was lower than that of P16 (1.08 ml/h) and TNF-α (0.38 ml/h). These findings were consistent with those of our earlier reports that showed that the $t_{1/2}$ of P16 and TNF-α was 5.76 and 33.6 min, respectively (16). These results suggested that the use of bare SC as a carrier can effectively lengthen the $t_{1/2}$ and caused a noticeable delay in the systemic CL of P16, thus indicating the potential of SC in clinical application.

Antitumor efficiency of SCP in mice bearing DU145 xenograft tumors

The therapeutic efficacy of SCP *in vivo* is an important index for its future medical application. Thus, we investigated the antitumor therapeutic efficacy of the different drug formulations in mice bearing DU145 xenograft tumors. Whereas tumors grew quickly in mice injected with NaCl, all of the drug formulations showed different extents of efficacy in tumor regression (**Fig. 8*A***). Although better suppression of tumor growth was achieved by free P16, Est, and TNF-α compared with NaCl, SCP exhibited

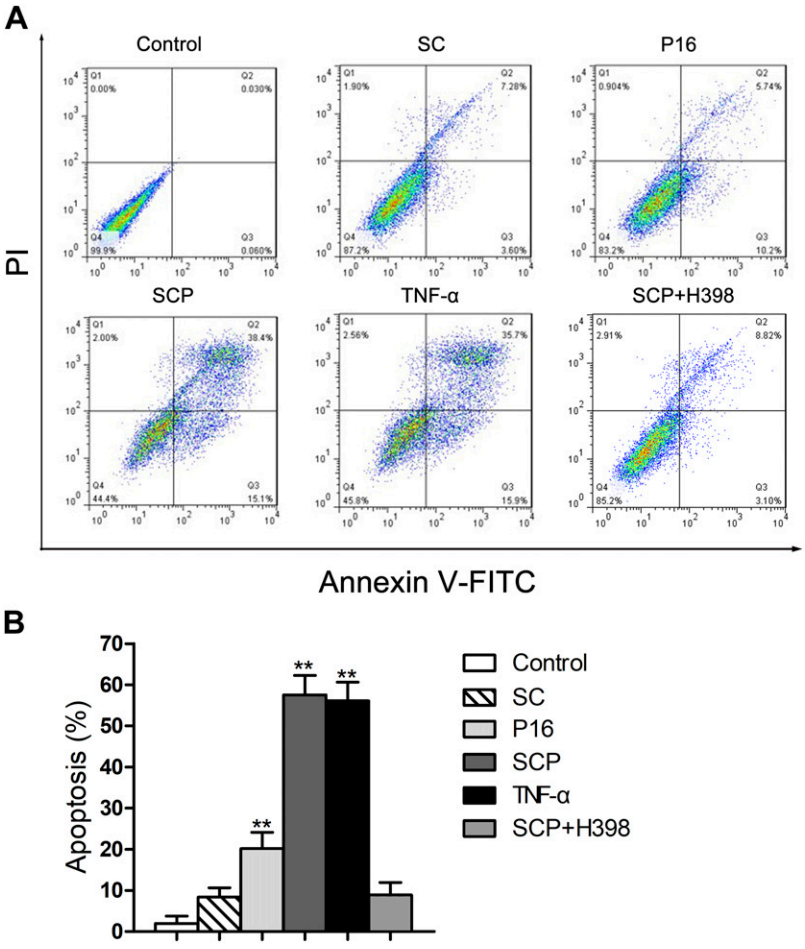

Figure 6. Apoptosis assays in DU145 cells by Annexin V-FITC/PI double staining. *A*) DU145 cells were treated with control (PBS), SC, P16, SCP, TNF-α, and SCP + H398. The apoptosis rates were evaluated using flow cytometric analyses. *B*) Statistics and data analysis of apoptosis in DU145 cell apoptosis. Each value represents the means ± SD of 3 separate experiments. $^{**}P < 0.01$, SCP *vs.* control or SC or P16 or SCP + H398; P16 *vs.* control; TNF-α *vs.* control.

the greatest inhibition efficacy on tumor growth ($P < 0.01$). At the end of the experiment, the tumor volume in mice treated with SCP was only 41.1% of the tumor volume in NaCl-injected mice and was 1.9-, 1.7-, and 1.1-fold smaller than the tumor volume in mice treated with free P16, Est, and TNF-α, respectively. Tumor samples were removed from mice at the end of the trial and were weighted (Fig. 8*B*, *C*). Tumors from mice that were treated with any of the drug formulations weighed significantly less than those from mice in the NaCl-treated group. The therapeutic efficacy was the highest for SCP (tumor inhibition of 64.3%) and was the next highest for TNF-α (58.2%), followed by Est (37.2%) and finally, P16 (23%). With the consideration that the antitumor efficacies of Est and TNF-α were hindered by concomitant systemic toxicities, it was necessary to evaluate the safety of SCP by monitoring changes in

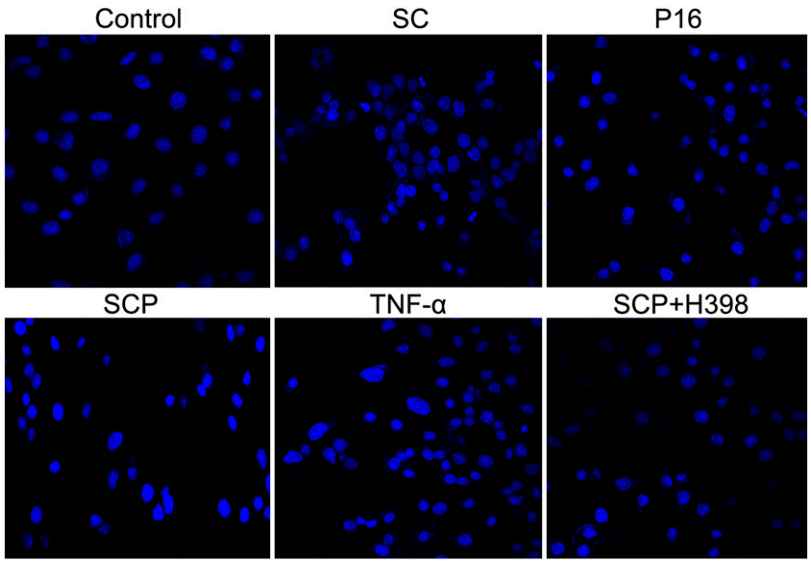

Figure 7. Apoptosis assays of DU145 cells by DAPI staining (original magnification, ×200). DU145 cells were treated with control (PBS), SC, P16, SCP, TNF-α, and SCP + H398. Representative nuclear morphologies of apoptotic cell nuclei were evaluated by DAPI staining.

TABLE 1. *Pharmacokinetic parameters of SCP, P16, and TNF-α in the plasma of BALB/c mice*

Parameter	Units	SCP		P16		TNF-α	
		Average	SD	Average	SD	Average	SD
Dose	mg/kg	5.00		5.00		5.00	
AUC	h × μg/ml	66.73*	1.22	4.65	1.86	13.00	2.23
$t_{\nu 2}$	h	13.52*	2.23	0.07	0.16	0.43	0.17
CL	ml/h	0.091*	0.02	1.08	0.001	0.38	0.046

*$P < 0.01$, SCP *vs.* P16 or TNF-α. Each value represents the mean ± SD of 3 separate experiments.

body weight (Fig. 8*D*). Treatment with SCP did not lead to any significant changes in body weight change during the course of study. This finding indicates the excellent tolerability of SCP regimens. In contrast, mice treated with Est and TNF-α lost 21 and 11.3% of their body weight, respectively, during the study period; this weight loss indicates serious systemic toxicity *in vivo*.

Low toxicity of SCP toward the liver and kidney *in vivo*

Furthermore, the analysis of hematologic biochemical indexes was performed to evaluate the cytotoxicity of SCP *in vivo*. There were no significant changes in the levels of ALT, AST, ALB, GLB, TBILI, DBILI, and IBILI between the SCP-treated and the CK group, thus indicating that SCP showed no obvious impact on liver function (**Table 2**). In contrast, treatment with Est and TNF-α markedly increased the levels of ALT and AST and significantly decreased the levels of ALB and A/G, which are importantly related to hepatopathy. This result indicated that Est and TNF-α might damage liver cells, thus influencing the protein synthesis. In addition, the BUN and CREA levels were not noticeably different between SCP-treated and CK mice, thus suggesting that SCP had negligible toxicity to kidney function. However, Est and TNF-α cause the damage to the kidney, as well as to the liver. Taken together, these results demonstrated that SCP possessed superior antitumor activity and much lower toxicity *in vivo* than Est and TNF-α, which supported its further application as a promising antitumor drug.

SCP inhibited proliferation and induced apoptosis in DU145 xenograft tumor tissue

Ki67, a biomarker of proliferation used for prognosis in a number of solid tumors, was used to determine the number of proliferative cells in DU145 tumor tissue. As shown in **Fig. 9*A***, the expression of Ki67 was widely distributed throughout the tumor tissue from the NaCl-treated mice, indicating robust tumor growth. However, the expression of Ki67 was dramatically lower in the tumors from mice treated with P16 and Est than in the tumors from mice in the NaCl group. Furthermore, Ki67 was barely detectable in the tumors from mice treated with SCP or TNF-α. Quantitative analysis of the images indicated

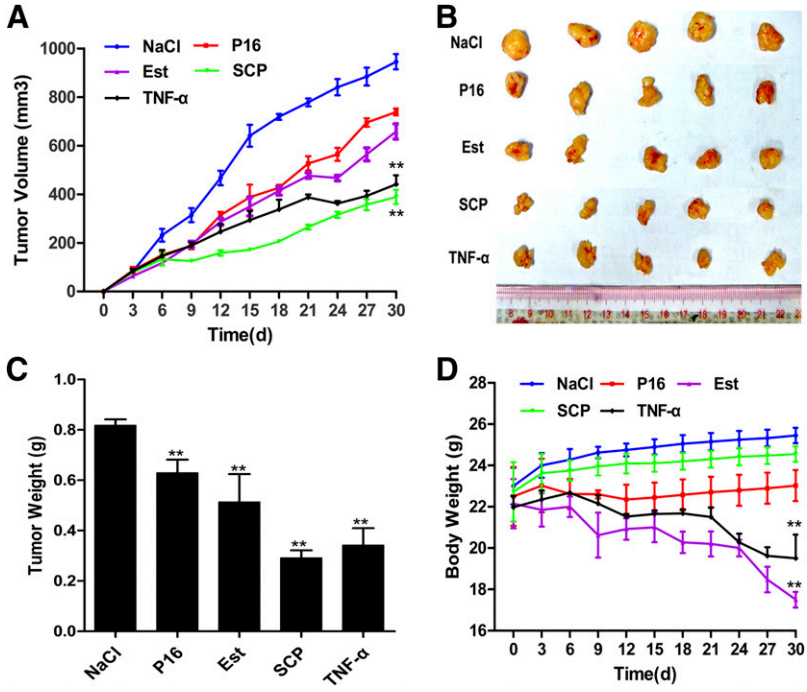

Figure 8. Antitumor efficiency of SCP *in vivo*. *A*) The tumor volume–time curve over 1 mo of the mouse DU145 xenograft tumor models treated with control (NaCl), P16, Est, SCP, and TNF-α. Data are means ± SD (each group, $n = 5$). **$P <$ 0.01, SCP or TNF-α *vs.* NaCl or P16 or Est. *B*) The tumors removed from BALB/c-nu/nu nude mice at the end of the experiment. *C*) The tumor weights were measured at the end of trial. Data are means ± SD (each group, $n = 5$). **$P < 0.01$, P16 or Est or SCP or TNF-α *vs.* NaCl. *D*) The body weight–time curve over 1 mo of treatment. Data are means ± SD (each group, $n = 5$). **$P < 0.01$, TNF-α or Est *vs.* NaCl or SCP or P16.

TABLE 2. *Hematologic analysis of tumor-bearing nude mice*

Biochemical index	BALB/c-nu/nu mice treatment					
	CK	NaCl	P16	Est	SCP	TNF-α
ALT (U/l)	36.46 ± 4.35	37 ± 3.35	36 ± 4.78	56 ± 8.08*	39 ± 3.67	69.5 ± 3.28*
AST (U/l)	98 ± 8.23	100 ± 7.17	95 ± 9.68	139 ± 10.39*	95 ± 5.99	114 ± 9.63*
ALB (g/l)	17.9 ± 3.8	17.5 ± 2.1	17.5 ± 0.69	15.05 ± 1.1*	16.5 ± 1.95	14.85 ± 2.37*
GLB (g/l)	40.73 ± 4.78	43.85 ± 5.45	41.45 ± 0.06	40.3 ± 0.12	40.17 ± 5.32	39.25 ± 2.37
A/G	0.42 ± 0.04	0.43 ± 0.01	0.41 ± 0.03	0.37 ± 0.02*	0.42 ± 0.08	0.37 ± 0.1*
BUN (mM)	12.93 ± 1.75	12.56 ± 2.18	11 ± 2.47	14.29 ± 1.86*	11.8 ± 2.15	10.5 ± 0.88
CREA (μM)	8.24 ± 1.23	8.17 ± 1.8	8.97 ± 0.46	12.78 ± 2.89*	9.05 ± 1.9	11.55 ± 1.73*
TBILI (μM)	12.3 ± 0.35	12.1 ± 0.16	13.1 ± 0.12	11.9 ± 0.12	11.5 ± 0.2	12.3 ± 0.29
DBILI (μM)	3.36 ± 1.89	3.45 ± 2.2	3.6 ± 2.54	3.79 ± 1.91	3.2 ± 2.1	3 ± 2.89
IBILI (μM)	8.9 ± 1.11	8.64 ± 1.02	9.5 ± 0.49	8.11 ± 0.8	9.3 ± 0.01	9.3 ± 0.17

Eight blood biochemical indexes (ALT, AST, ALB, GLB, A/G, TBILI, DBILI, and IBILI) that were closely relevant to the liver function were analyzed. Two blood biochemical indexes (BUN and CREA) that were closely relevant to the kidney function were analyzed. *$P < 0.01$, Est or TNF-α *vs.* SCP or CK or NaCl. Each value represents the mean ± SD of 3 separate experiments.

that the rate of proliferation in the SCP -treated group was significantly lower than that in the NaCl-treated group (Fig. 9*B*). These data were consistent with the tumor growth curve as measured by tumor size, thus indicating that SCP suppressed tumor growth *in vivo* by inhibiting tumor cell proliferation.

TUNEL assay

Apoptotic cells in DU145 xenograft tumors were further analyzed by a TUNEL assay. TUNEL can detect the early stage of DNA fragmentation in apoptotic cells before changes in morphology. We examined the amount of green fluorescence, which represented the labeling of apoptotic cells with dUTP, and blue fluorescence, which represented nuclei stained with DAPI. The various drug formulations caused varying degrees of tumor cell apoptosis, consistent with the results of the *in vivo* antitumor efficacy study (**Fig. 10*A***). Tumors from mice treated with SCP showed a higher intensity of green fluorescence than did tumors from mice treated with other formulations. A much lower but still abundant amount of green fluorescence was visible in tumors from mice treated with TNF-α. In contrast, green fluorescence was barely detectable in tumors from mice treated with NaCl. Quantitative analysis of the images indicated that the rate of apoptosis in the tumors from mice in the SCP-treated group was significantly higher than that in the tumors from mice in the other groups (Fig. 10*B*). Taken together, the results of the Ki67 immunofluorescence and TUNEL assays revealed that the antitumor effect of SCP was mainly caused by the inhibition of cell proliferation and the promotion of cell apoptosis.

SCP-mediated induction of the p38 MAPK/JNK signaling pathway *in vivo*

Much evidence has supported that apoptosis can be induced through diverse signaling pathways, for instance, the MAPK and AKT pathways (30, 31). The MAPK cascade, which includes p38, JNK, and ERK, can combine extracellular signals and cause cell apoptosis (32). Given the importance of the MAPK pathway in cancer cell survival and apoptosis, we examined the phosphorylated (activated) forms of the kinases in the tumors of treated mice by Western blotting. SCP treatment significantly increased the levels of phosphorylated p38 and JNK, whereas it had no impact on the expression levels of total p38 and JNK in cells undergoing apoptosis (**Fig. 11**). Our results indicated that the regulation of p38 and JNK phosphorylation was relevant to SCP-induced cell death.

Effect of SCP on cell-cycle-associated proteins in DU145 xenograft nude mice

Different regulators, such as cyclins, cyclin-dependent kinases (CDKs), CDK inhibitors (CKIs), and growth-suppressor genes, working in multiple pathways, tightly regulated control of the cell cycle. As SCP treatment arrested DU145 cells in the G_0/G_1 phase *in vitro*, we evaluated the levels of cell-cycle-associated regulators related to this function *in vivo*. It was found by Western blotting that SCP treatment significantly reduced the expression levels of DNA-binding 2 (Id2) and cyclin E and the CDKs CDK2 (**Fig. 12*A***). The Rb pathway is associated with cell progression from the G_1 phase to the S phase. The phosphorylation of the Rb protein may be induced by cyclin-CDK complexes; phosphorylated Rb protein then facilitates the release of the E2F1 transcription factor, thus resulting in S-phase entry (33). As SCP treatment noticeably reduced the levels of phosphorylated Rb and E2F1 in DU145 xenograft cells, E2F1 failed to release from Rb, resulting in G_0/G_1 arrest. Furthermore, the expression levels of CKIs, such as p21, p27, and p53, regulated the progression of the cell cycle in the G_1 phase. As shown in Fig. 12*B*, the protein levels of p21, p27, and p53 were obviously increased by SCP treatment. Taken together, these data suggested that these proteins were associated with the G_0/G_1-phase arrest induced by SCP.

Effect of SCP on apoptosis-associated proteins in DU145 xenograft nude mice

In the caspase cascade signaling cascade, caspase-8 (an initiator caspase, extrinsic Fas/TNF mediated) and caspase-3 (an effector caspase) are proteases deemed to be significant in the triggering of cell apoptosis after they are cleaved (34).

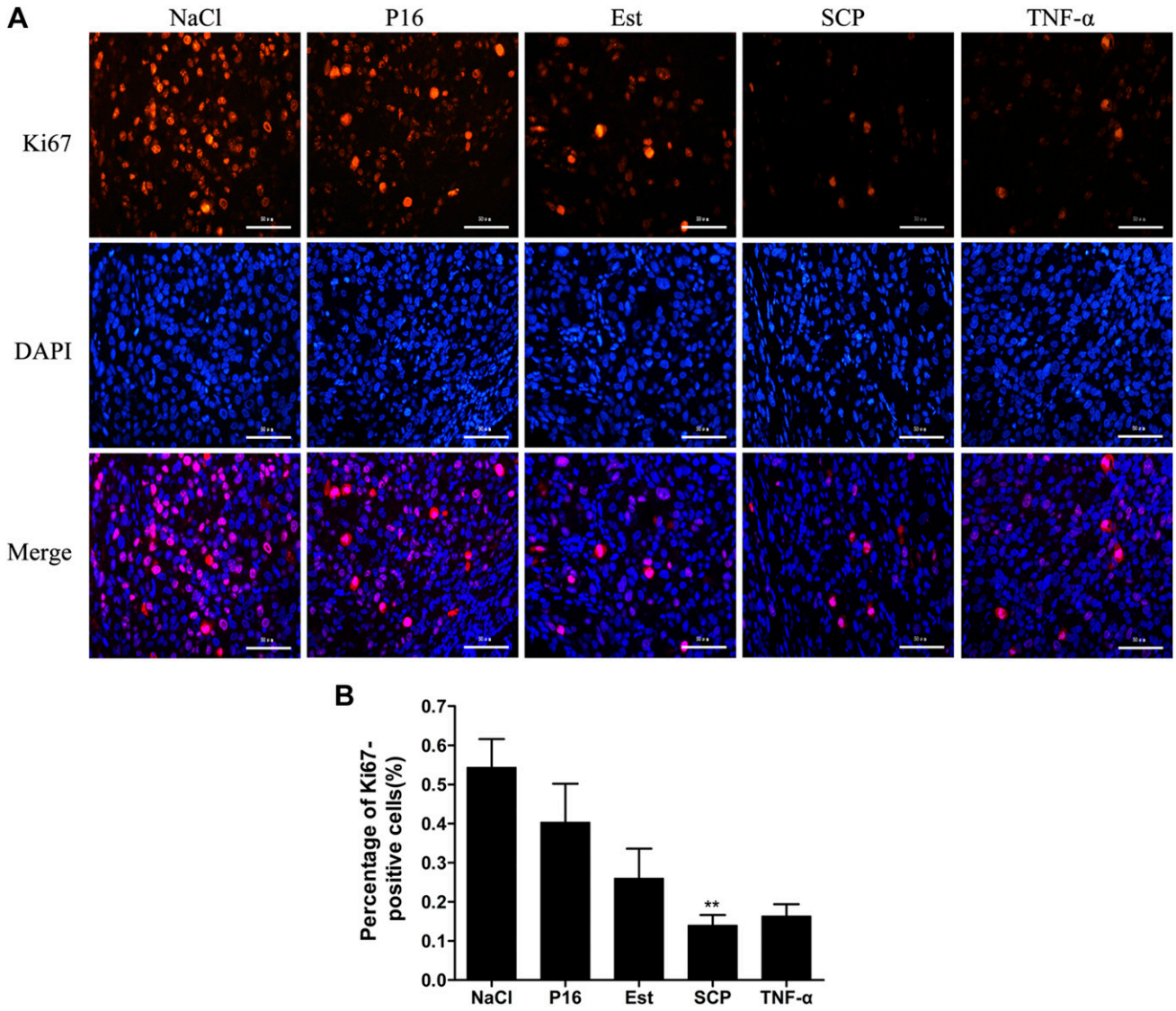

Figure 9. SCP inhibited cell proliferation in DU145 xenograft tumors, as demonstrated by Ki67 staining (original magnification, ×400). *A*) Tumor sections harvested from mice subcutaneously injected with NaCl (control), P16, Est, and SCP. Representative images show proliferating cells (rad fluorescence) and the corresponding cell nuclei (blue fluorescence). *B*) Quantification of the Ki67-positive cells in *A*. $^{**}P < 0.01$, SCP *vs.* NaCl or P16 or Est or TNF-α. Each value represents means ± SD of 3 separate experiments.

In the course of the cell apoptosis experiment *in vitro*, we observed that SCP noticeably increased DU145 cell apoptosis (Figs. 6 and 7). Nevertheless, the molecular mechanisms of the apoptosis-inducing action of SCP remained to be elucidated. To investigate whether apoptosis was the major pattern of cell death induced by SCP *in vivo*, we examined the activation of 2 apoptotic markers, namely, caspase-8 and caspase-3, in NaCl-, P16-, SCP-, TNF-α-, and Est-treated mice bearing DU145 xenograft tumors. As shown in **Fig. 13**, the cleavage of caspase-8 and caspase-3 was markedly elevated in the tumor of mice treated with SCP, which demonstrated that the apoptotic effect of SCP was associated with a caspase-dependent pathway. In addition, TNF-α induced the activation of these 2 apoptotic markers. Hence, it was conjectured that the activation of cell apoptosis-regulating signals by SCP may be relevant to the activation of signaling in a caspase cascade similar to the TNF-α-mediated apoptosis pathway.

DISCUSSION

Prostate cancer is a major cause of morbidity and mortality in men worldwide, and the etiology of prostate cancer remains unknown. Despite the availability of some kinds of chemotherapeutic agents for prostate cancer treatment, problems, such as intolerable side-effects, short $t_{1/2}$, poor aqueous solubility, and low oral bioavailability of the agents, still represent the chief challenges in prostate cancer treatment (35). Because of the unsatisfactory nature of the conventional treatments for prostate cancer, it is urgent to develop a novel, efficient chemotherapeutic agent for treating this cancer. Among various strategies that could be used to conquer these challenges, nanotechnology has emerged as a promising candidate.

NPs are commonly composed of thousands of atoms and possess particular physical and biochemical properties, including a large surface area for loading chemotherapeutic

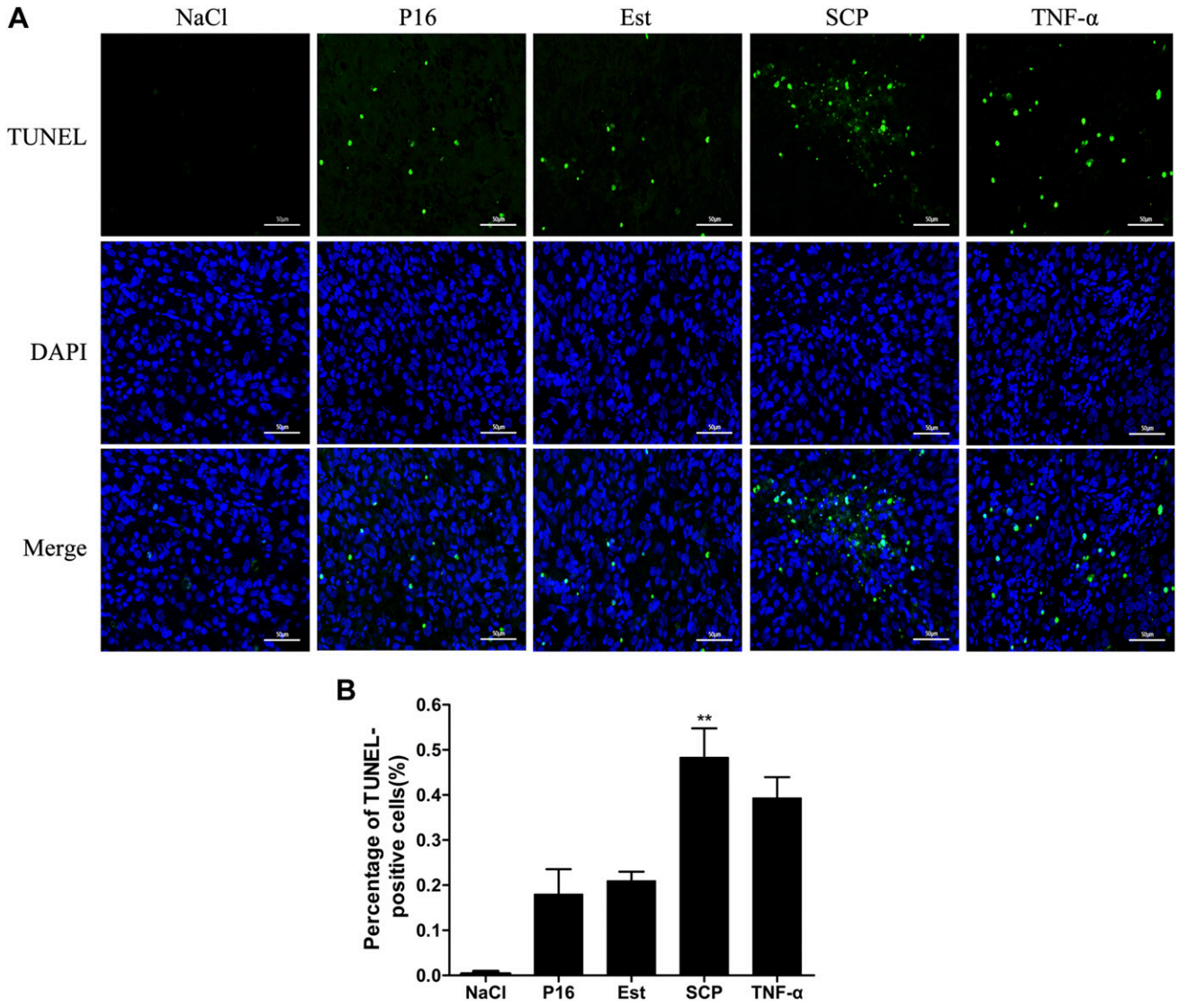

Figure 10. Apoptotic cells in DU145 xenograft tumors were detected by a TUNEL assay (original magnification, ×400). *A*) Tumor sections harvested from mice subcutaneously injected with NaCl (control), P16, Est, SCP, and TNF-α. Representative images show apoptotic cells (green fluorescence) and the corresponding cell nuclei (blue fluorescence). *B*) Quantification of the apoptosis-positive cells in *A*. $^{**}P < 0.01$, SCP *vs.* NaCl or P16 or Est or TNF-α. Each value represents the means ± SD of 3 separate experiments.

agents. As the length of NPs is <200 nm, they can be encapsulated with therapeutic drugs and then injected into blood vessels without concern for embolization. At this length scale, NPs have the potential to penetrate and deliver throughout different tissues, bind to cell-surface receptors, enter target cells for the intracellular delivery of their payloads, and impact intracellular signaling pathways. These NP–drug formulations increase the specificity, tolerability, and therapeutic index of relevant drugs (36, 37). Recently, several antitumor drugs and bioactive peptides have been successfully encapsulated in NPs to increase their sustained release time and antitumor effects (38, 39). Cisplatin is widely used in the treatment of solid tumors. Nevertheless, cisplatin exhibits dose-limiting side-effects, such as nephrotoxicity, neurotoxicity, and gastrointestinal disturbance, thus hindering its clinical application (40). Hence, Farokhzad and coworkers (41) encapsulated cisplatin in aptamer-targeted poly(D,L-lactic-co-glycolic acid)-b-poly(ethylene glycol) NPs to overcome these disadvantages. They found that compared with free cisplatin, these NP-drug formulations significantly improved the therapeutic index and markedly decreased the nephrotoxicity of the drugs in LNCaP xenograft mice (41). Likewise, several therapeutic NP-based drugs for prostate cancer have been reported (42–46). As a critical cytokine that causes tumor cell necrosis and apoptosis, TNF-α is a potential molecule for use in cancer treatment. Therefore, based on the understanding of NP-mediated drug-delivery systems, we intended to enhance the antitumor effects of TNF-α and decreased its side-effects *via* nanotechnology for the treatment of prostate cancer.

TNF-α was first discovered as an antitumor cytokine that triggers hemorrhagic necrosis. It is well known that TNF-α can selectively destroy tumor-associated vessels. Preclinical trials have identified the potent antitumor effects of TNF-α both in syngeneic murine tumor models

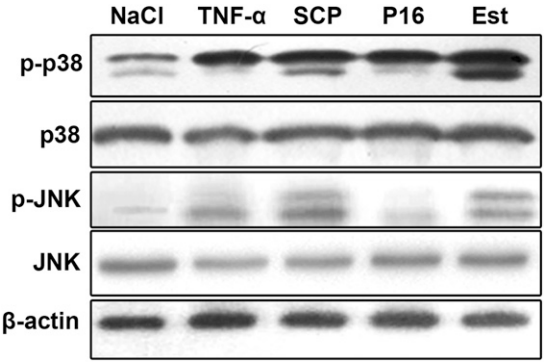

Figure 11. Effects of SCP on the phosphorylation (p) status and expression levels of p38 and JNK in DU145 xenograft nude mice. The expression levels of p-p38, p38, p-JNK, and JNK were analyzed by Western blotting assay. β-Actin was used as the loading control. The protein bands are representatives of 3 separate experiments with similar results.

and in human tumor xenografts in nude mice (47, 48). Unfortunately, the clinical use of TNF-α for systemic treatment has been hindered by a wide spectrum of systemic toxicities. To increase the antitumor efficacy and decrease the toxicity of TNF-α, scientists have been actively engaged in designing TNF-α derivatives. Yan *et al.* (49) prepared a recombinant TNF-α mutant (rmhTNF-α) *via* deletion of the first 7 aa from the N-terminus and replacement of 4 aa (Pro8Arg, Ser9Lys, Asp10Arg, and Leu157Phe). The rmhTNF-α construct exhibited an antitumor efficacy 25 times higher than that of wild-type TNF-α and a median lethal dose at least 50 times higher than that of wild-type TNF-α in different xenograft nude mouse models (49). Subsequently, the clinical trials also demonstrated that the novel rmhTNF-α construct possessed high antitumor efficiency and low systemic toxicity (50). Additionally, Kuroda *et al.* (51) reported that a mutant of human TNF-α (V29), in which Arg29 was substituted with Val (Arg29Val), exhibited higher antitumor efficiency and lower toxicity than did wild-type TNF-α. As its affinity for TNFR2 was greatly decreased compared with its affinity for TNFR1, the V29 mutant might be a useful antitumor agent (51). Furthermore, several investigations have revealed that the antitumor effects of TNF-α were primarily regulated by TNFR1, whereas the toxicity and side-effects were primarily regulated by TNFR2 (52–54).

P16 is a 20 aa bioactive peptide derived from TNF-α, which included amino acid residues 75–94. We previously used gene-engineering technology to construct a 31 aa recombinant peptide, namely, RMP16, by addition of a specific human serum ALB-binding 7-mer (WQRPSSW) at the N-terminus, followed by a sustained-release linker (−IEGR−) that was sensitively recognized by plasma factor Xa, along with the 20 aa TNF-α–derived peptide P16. RMP16 could slowly release P16 into the circulation and displayed powerful antitumor effects through selectively binding to TNFR1 (16). In the present investigation, we have successfully developed a novel TNF-α–derived peptide, namely, SCP, by nanotechnology; SCP comprises P16, which selectively binds to TNFR1 with SC as a sustained-release carrier. SC not only slowly released the bioactive peptide P16 in an orderly manner *via* specific cleavage by cathepsin D and chymotrypsin but also slightly suppressed tumor cell growth and caused apoptosis. Therefore, SC usually functions as a drug-delivery carrier and an auxiliary therapeutic agent. *In vitro*, SCP effectively inhibited cancer cell growth and demonstrated high selectivity between cancer and normal cells. This effect was likely attributable to cell-line variations and discrepancies in molecular characteristics (55, 56). SCP induced the apoptosis of DU145 prostate cancer cells *via* the selective activation of TNFR1 compared with TNF-α. The results of DAPI staining in DU145 cells incubated with different formulations showed that SCP could cause distinct damages to DU145 cells, including chromatin condensation and nuclear condensation associated with apoptosis.

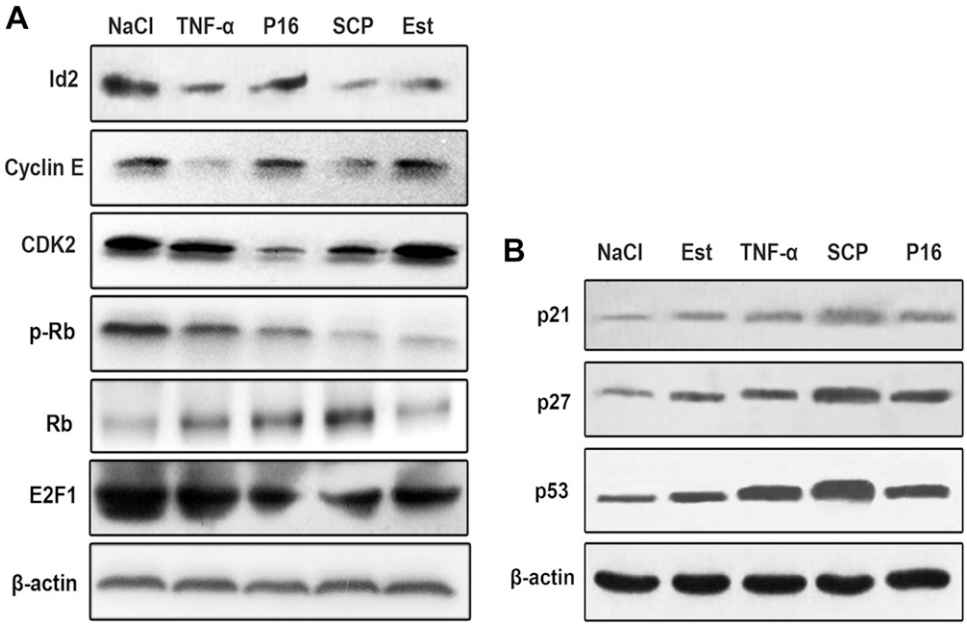

Figure 12. Effects of SCP on cell-cycle-related proteins in DU145 xenograft-implanted nude mice. *A*) The expression of cell-cycle-related proteins, such as Id2, cyclin E, CDK2, p-Rb, Rb, and E2F1, was analyzed by Western blotting. *B*) The expression of p21, p27, and p53 was analyzed by Western blotting. β-Actin was used as the loading control. The protein bands are representative of 3 separate experiments with similar results.

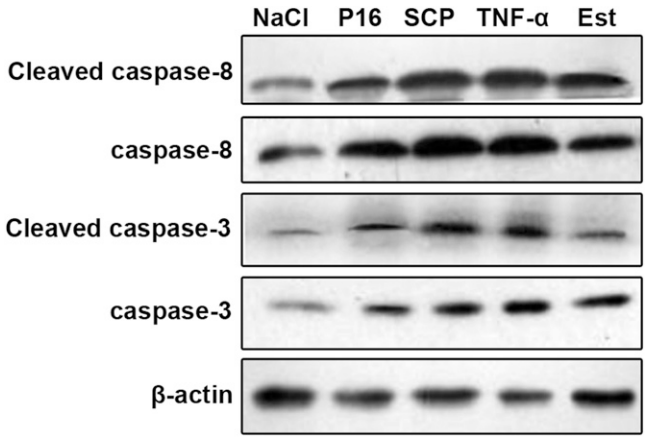

Figure 13. SCP activates intracellular apoptotic signaling pathways in DU145 xenograft nude mice. The expression of cleaved caspase-8, caspase-8, cleaved caspase-3, and caspase-3 was analyzed by Western blotting. β-Actin was used as the loading control. The protein bands are representative of 3 separate experiments with similar results.

The aforementioned potent antitumor effects of SCP *in vitro* encouraged us to investigate the antitumor effects in DU145 xenograft mice. The $t_{1/2}$ of SCP was longer than that of P16 and TNF-α *in vivo*. SCP could significantly inhibit tumor growth in nude mice without resulting in weight loss. In addition, analysis of hematologic biochemical indexes revealed that SCP did not cause damages to the liver or kidney of tumor-bearing nude mice after continuous administration for 1 mo. Although TNF-α and Est (the clinical drug for prostate cancer treatment) had remarkable antitumor effects in tumor-bearing nude mice, mice treated with these agents displayed apparent weight loss and poor appetite or spirit, and the hematologic biochemical indexes indicated that TNF-α and Est could cause damages to liver and kidney tissue, respectively. Moreover, P16 only slightly suppressed tumor growth without damage to liver and kidney tissue. In addition to this finding, the Ki67 staining and the TUNEL assay showed that SCP suppressed tumor cell proliferation and induced apoptosis in xenograft tumors. The results of the *in vivo* study agreed with those of the *in vitro* experiment, thus suggesting that the prominent antitumor effects might be responsible for the cytotoxicity of SCP. Taken together, these observations collectively shed light on the fact that SCP exhibited a pronounced antitumor profiles *in vivo*.

In further studies, we investigated the molecular mechanisms of underlying the antitumor effects of SCP in DU145 xenograft nude mice. CDKs are the central components controlling the initiation, progression, and completion of cell division (57). In particular, the progression of the cell cycle from the G_1/G_0 phase to the S phase is regulated by CDK2, and excessive CDK2 activity is associated with the deregulated cell proliferation in tumors (58). Therefore, CDK2 inhibitors are potentially effective antitumor agents. p21 and p27 are 2 main CKIs; they regulate CDK2 activity by binding to cyclin-CDK complexes, thereby inhibiting the catalytic activity of CDK2 (59). Another tumor-suppressor protein, namely, p53, acts as a transcription factor that regulates the expression of various genes relevant to cell-cycle arrest and apoptosis (60). In the present study, we found that SCP treatment significantly increased the expression levels of p21, p27, and p53. Additionally, inhibitor of Id2 is a proproliferative gene and a marker for human prostate cancer progression, and it was overexpressed in highly aggressive prostate cancer cells *in vivo* (61). Consistent with those of previous study, our results showed that Id2 expression was directly repressed by p53 (62). With regard to the important roles played by the cell-cycle-associated proteins Rb and E2F1 in regulating cell-cycle progression from the G_1/G_0 phase to the S phase (63), we investigated the effects of SCP on these targets. SCP treatment could inhibit E2F1 release from cyclin-CDK complexes by decreasing the phosphorylation of Rb. These observations collectively indicated that SCP arrested prostate cancer cells at the G_0/G_1 phase *in vivo* through the upregulation of p21, p27, and p53 and the downregulation of CDK-2, cyclin E, Id2, p-Rb, and E2F1.

Apoptosis is a physiologic process that is crucial for organisms to maintain tissue homeostasis and eliminate harmful or unnecessary cells. Most of the current cytotoxic antitumor drugs exert their effects by the induction of apoptosis in cancer cells (64). Caspases, as a highly conserved family of cysteine proteases, have been found to play a crucial role in the initiation and execution of apoptosis in various biologic systems (65). Caspase-3 has been considered as the central regulator of apoptosis, whereas caspase-8 functions as an initiator of death receptor-mediated apoptotic pathways (66). Consistent with the results obtained in cell models, SCP treatment caused the upregulation of cleaved caspase-8 and cleaved caspase-3 but only a relatively small change in caspase-8 and caspase-3 expression. To elucidate the events upstream of SCP-mediated apoptosis, the expression of pivotal apoptosis-correlated proteins was investigated in tumor tissues. Our results suggested that SCP dramatically increased the phosphorylation of p38 and JNK, whereas SCP did not affect the expression levels of total p38 and JNK in apoptotic cells. Taken together, these findings revealed that SCP exhibited an excellent antitumor therapeutic effect *in vivo* by inducing apoptosis.

In summary, we developed a novel SCP delivery system with satisfactory EE and LE. SCP was able to release P16 in a sustained manner *in vitro* and showed a greater ability than the equivalent dose of P16 to inhibit DU145 cell proliferation selectively, arrest the cell cycle, and induce cell apoptosis. In DU145 xenograft mouse models, SCP noticeably inhibited tumor growth without measurable adverse effects than did free p16. Further mechanistic studies revealed that SCP can inhibit tumor growth in DU145 xenograft mouse models through its effects on the p38 MAPK/JNK signaling pathway, G_0/G_1 cell-cycle arrest, and the caspase-dependent apoptosis pathway. Although more studies are necessary to understand the mechanisms underlying the antitumor effects of SCP, our data form a foundation for the exploration of this nanodrug formulation as an effective candidate drug for human prostate cancer chemotherapy. FJ

ACKNOWLEDGMENTS

The authors thank the Key Laboratory of Bioengineering Medicine of Guangdong Province, Jinan University, and the

Center for Reproductive Medicine, The Sixth Affiliated Hospital of Guangzhou Medical University. The authors also thank American Journal Experts for the English language editing. This work was supported by the National Natural Science Foundation of China (Grants 81741130 and 81373314); Natural Science Foundation of Guangdong Province (Grant 2015A030313333); Science and Technology Planning Project of Guangdong Province (Grants 2014A020210015 and 2013B090500105); Guangzhou Municipal Science and Technology Program (Grants 201707010245 and 201704020117); and Medical Research Foundation of Guangdong Province (Grant B2014426). The authors declare no conflicts of interest.

AUTHOR CONTRIBUTIONS

A. Hong and Y. Ma designed research; Q. Yan, X. Chen, H. Gong, P. Qiu, X. Xiao, and S. Dang assisted with the data collection and performed research; Q. Yan and Y. Ma contributed to the writing of the manuscript; A. Hong contributed to editing of the manuscript; and X. Chen and H. Gong conducted the data analysis.

REFERENCES

1. Torre, L. A., Bray, F., Siegel, R. L., Ferlay, J., Lortet-Tieulent, J., and Jemal, A. (2015) Global cancer statistics, 2012. *CA Cancer J. Clin.* **65**, 87–108
2. Sandhu, G. S., Nepple, K. G., Tanagho, Y. S., and Andriole, G. L. (2013) Prostate cancer chemoprevention. *Semin. Oncol.* **40**, 276–285
3. Lacy, J. M., and Kyprianou, N. (2014) A tale of two trials: the impact of 5α-reductase inhibition on prostate cancer (Review). *Oncol. Lett.* **8**, 1391–1396
4. Li, J., Sharkey, C. C., Huang, D., and King, M. R. (2015) Nanobiotechnology for the therapeutic targeting of cancer cells in blood. *Cell. Mol. Bioeng.* **8**, 137–150
5. Ohtani, T., Nakamura, T., Toda, K., and Furukawa, F. (2006) Cyclophosphamide enhances TNF-alpha-induced apoptotic cell death in murine vascular endothelial cell. *FEBS Lett.* **580**, 1597–1600
6. Bergers, G., and Benjamin, L. E. (2003) Tumorigenesis and the angiogenic switch. *Nat. Rev. Cancer* **3**, 401–410
7. Pennica, D., Nedwin, G. E., Hayflick, J. S., Seeburg, P. H., Derynck, R., Palladino, M. A., Kohr, W. J., Aggarwal, B. B., and Goeddel, D. V. (1984) Human tumour necrosis factor: precursor structure, expression and homology to lymphotoxin. *Nature* **312**, 724–729
8. Chu, W. M. (2013) Tumor necrosis factor. *Cancer Lett.* **328**, 222–225
9. Wiens, G. D., and Glenney, G. W. (2011) Origin and evolution of TNF and TNF receptor superfamilies. *Dev. Comp. Immunol.* **35**, 1324–1335
10. Speeckaert, M. M., Speeckaert, R., Laute, M., Vanholder, R., and Delanghe, J. R. (2012) Tumor necrosis factor receptors: biology and therapeutic potential in kidney diseases. *Am. J. Nephrol.* **36**, 261–270
11. Idriss, H. T., and Naismith, J. H. (2000) TNF alpha and the TNF receptor superfamily: structure-function relationship(s). *Microsc. Res. Tech.* **50**, 184–195
12. Fontaine, V., Mohand-Said, S., Hanoteau, N., Fuchs, C., Pfizenmaier, K., and Eisel, U. (2002) Neurodegenerative and neuroprotective effects of tumor necrosis factor (TNF) in retinal ischemia: opposite roles of TNF receptor 1 and TNF receptor 2. *J. Neurosci.* **22**, RC216
13. Gordon, R., Anantharam, V., Kanthasamy, A. G., and Kanthasamy, A. (2012) Proteolytic activation of proapoptotic kinase protein kinase Cδ by tumor necrosis factor α death receptor signaling in dopaminergic neurons during neuroinflammation. *J. Neuroinflammation* **9**, 82
14. Liu, R., Xi, L., Luo, D., Ma, X., Yang, W., Xi, Y., Wang, H., Qian, M., Fan, L., Xia, X., Li, K., Wang, D., Zhou, J., Meng, L., Wang, S., and Ma, D. (2012) Enhanced targeted anticancer effects and inhibition of tumor metastasis by the TMTP1 compound peptide TMTP1-TAT-NBD. *J. Control. Release* **161**, 893–902
15. Zhang, X. M., Weber, I., and Chen, M. J. (1992) Site-directed mutational analysis of human tumor necrosis factor-alpha receptor binding site and structure-functional relationship. *J. Biol. Chem.* **267**, 24069–24075
16. Ma, Y., Zhao, S., Shen, S., Fang, S., Ye, Z., Shi, Z., and Hong, A. (2015) A novel recombinant slow-release TNF α-derived peptide effectively inhibits tumor growth and angiogensis. *Sci. Rep.* **5**, 13595
17. Chauhan, V. P., and Jain, R. K. (2013) Strategies for advancing cancer nanomedicine. *Nat. Mater.* **12**, 958–962
18. Shi, J., Votruba, A. R., Farokhzad, O. C., and Langer, R. (2010) Nanotechnology in drug delivery and tissue engineering: from discovery to applications. *Nano Lett.* **10**, 3223–3230
19. Yuan, Y. G., Peng, Q. L., and Gurunathan, S. (2017) Silver nanoparticles enhance the apoptotic potential of gemcitabine in human ovarian cancer cells: combination therapy for effective cancer treatment. *Int. J. Nanomedicine* **12**, 6487–6502
20. Wang, Z., Xu, B., Zhang, L., Zhang, J., Ma, T., Zhang, J., Fu, X., and Tian, W. (2013) Folic acid-functionalized mesoporous silica nanospheres hybridized with AIE luminogens for targeted cancer cell imaging. *Nanoscale* **5**, 2065–2072
21. Rastogi, V., Yadav, P., Bhattacharya, S. S., Mishra, A. K., Verma, N., Verma, A., and Pandit, J. K. (2014) Carbon nanotubes: an emerging drug carrier for targeting cancer cells. *J. Drug Deliv.* **2014**, 670815
22. Wang, H., Zhang, J., and Yu, H. (2007) Elemental selenium at nano size possesses lower toxicity without compromising the fundamental effect on selenoenzymes: comparison with selenomethionine in mice. *Free Radic. Biol. Med.* **42**, 1524–1533
23. Zhang, J., Wang, X., and Xu, T. (2008) Elemental selenium at nano size (Nano-Se) as a potential chemopreventive agent with reduced risk of selenium toxicity: comparison with se-methylselenocysteine in mice. *Toxicol. Sci.* **101**, 22–31
24. Prabaharan, M. (2015) Chitosan-based nanoparticles for tumor-targeted drug delivery. *Int. J. Biol. Macromol.* **72**, 1313–1322
25. Liu, J., Liu, J., Xu, H., Zhang, Y., Chu, L., Liu, Q., Song, N., and Yang, C. (2014) Novel tumor-targeting, self-assembling peptide nanofiber as a carrier for effective curcumin delivery. *Int. J. Nanomedicine* **9**, 197–207
26. Liu, W., Li, X., Wong, Y. S., Zheng, W., Zhang, Y., Cao, W., and Chen, T. (2012) Selenium nanoparticles as a carrier of 5-fluorouracil to achieve anticancer synergism. *ACS Nano* **6**, 6578–6591
27. Dennis, M. S., Zhang, M., Meng, Y. G., Kadkhodayan, M., Kirchhofer, D., Combs, D., and Damico, L. A. (2002) Albumin binding as a general strategy for improving the pharmacokinetics of proteins. *J. Biol. Chem.* **277**, 35035–35043
28. Zhao, S. J., Wang, D. H., Li, Y. W., Han, L., Xiao, X., Ma, M., Wan, D. C., Hong, A., and Ma, Y. (2017) A novel selective VPAC2 agonist peptide-conjugated chitosan modified selenium nanoparticles with enhanced anti-type 2 diabetes synergy effects. *Int. J. Nanomedicine* **12**, 2143–2160
29. Zhang, Y., Li, X., Huang, Z., Zheng, W., Fan, C., and Chen, T. (2013) Enhancement of cell permeabilization apoptosis-inducing activity of selenium nanoparticles by ATP surface decoration. *Nanomedicine (Lond.)* **9**, 74–84
30. Liu, T., Zeng, L., Jiang, W., Fu, Y., Zheng, W., and Chen, T. (2015) Rational design of cancer-targeted selenium nanoparticles to antagonize multidrug resistance in cancer cells. *Nanomedicine (Lond.)* **11**, 947–958
31. Zhang, Y., Zheng, S., Zheng, J. S., Wong, K. H., Huang, Z., Ngai, S. M., Zheng, W., Wong, Y. S., and Chen, T. (2014) Synergistic induction of apoptosis by methylseleninic acid and cisplatin, the role of ROS-ERK/AKT-p53 pathway. *Mol. Pharm.* **11**, 1282–1293
32. Wang, N., Feng, Y., Zeng, L., Zhao, Z., and Chen, T. (2015) Functionalized multiwalled carbon nanotubes as carriers of ruthenium complexes to antagonize cancer multidrug resistance and radioresistance. *ACS Appl. Mater. Interfaces* **7**, 14933–14945
33. Fang, X. Y., and Ye, D. Q. (2014) E2F1: a potential therapeutic target for systematic lupus erythematosus. *Rheumatol. Int.* **34**, 1175–1176
34. Errami, Y., Naura, A. S., Kim, H., Ju, J., Suzuki, Y., El-Bahrawy, A. H., Ghonim, M. A., Hemeida, R. A., Mansy, M. S., Zhang, J., Xu, M., Smulson, M. E., Brim, H., and Boulares, A. H. (2013) Apoptotic DNA fragmentation may be a cooperative activity between caspase-activated deoxyribonuclease and the poly(ADP-ribose) polymerase-regulated DNAS1L3, an endoplasmic reticulum-localized endonuclease that translocates to the nucleus during apoptosis. *J. Biol. Chem.* **288**, 3460–3468
35. Shen, M. M., and Abate-Shen, C. (2010) Molecular genetics of prostate cancer: new prospects for old challenges. *Genes Dev.* **24**, 1967–2000
36. Li, Y., Cui, T., Kong, X., Yi, X., Kong, D., Zhang, J., Liu, C., and Gong, M. (2018) Nanoparticles induced by embedding self-assembling cassette into glucagon-like peptide 1 for improving in vivo stability. *FASEB J.*, **32**, 2992–3004
37. Devalliere, J., Chang, W. G., Andrejecsk, J. W., Abrahimi, P., Cheng, C. J., Jane-wit, D., Saltzman, W. M., and Pober, J. S. (2014) Sustained delivery of proangiogenic microRNA-132 by nanoparticle transfection improves endothelial cell transplantation. *FASEB J.* **28**, 908–922

38. Kulhari, H., Pooja, D., Shrivastava, S., Telukutala, S. R., Barui, A. K., Patra, C. R., Naidu Vegi, G. M., Adams, D. J., and Sistla, R. (2015) Cyclic-RGDfK peptide conjugated succinoyl-TPGS nanomicelles for targeted delivery of docetaxel to integrin receptor over-expressing angiogenic tumours. *Nanomedicine (Lond.)* **11**, 1511–1520
39. Pritchard, T., Rosengren, R. J., Greish, K., and Taurin, S. (2016) Raloxifene nanomicelles reduce the growth of castrate-resistant prostate cancer. *J. Drug Target.* **24**, 441–449
40. Sánchez-González, P. D., López-Hernández, F. J., López-Novoa, J. M., and Morales, A. I. (2011) An integrative view of the pathophysiological events leading to cisplatin nephrotoxicity. *Crit. Rev. Toxicol.* **41**, 803–821
41. Dhar, S., Kolishetti, N., Lippard, S. J., and Farokhzad, O. C. (2011) Targeted delivery of a cisplatin prodrug for safer and more effective prostate cancer therapy in vivo. *Proc. Natl. Acad. Sci. USA* **108**, 1850–1855
42. Castro Nava, A., Cojoc, M., Peitzsch, C., Cirillo, G., Kurth, I., Fuessel, S., Erdmann, K., Kunhardt, D., Vittorio, O., Hampel, S., and Dubrovska, A. (2015) Development of novel radiochemotherapy approaches targeting prostate tumor progenitor cells using nanohybrids. *Int. J. Cancer* **137**, 2492–2503
43. Yan, J., Wang, Y., Zhang, X., Liu, S., Tian, C., and Wang, H. (2016) Targeted nanomedicine for prostate cancer therapy: docetaxel and curcumin co-encapsulated lipid-polymer hybrid nanoparticles for the enhanced anti-tumor activity *in vitro* and *in vivo*. *Drug Deliv.* **23**, 1757–1762
44. Khan, N., Bharali, D. J., Adhami, V. M., Siddiqui, I. A., Cui, H., Shabana, S. M., Mousa, S. A., and Mukhtar, H. (2014) Oral administration of naturally occurring chitosan-based nanoformulated green tea polyphenol EGCG effectively inhibits prostate cancer cell growth in a xenograft model. *Carcinogenesis* **35**, 415–423
45. Chen, B., Pan, R., Askhatova, D., and Chen, P. (2015) Effective small interfering RNA delivery *in vitro* via a new stearylated cationic peptide. *Int. J. Nanomedicine* **10**, 3303–3314
46. Yang, Q., Yang, Y., Li, L., Sun, W., Zhu, X., and Huang, Y. (2015) Polymeric nanomedicine for tumor-targeted combination therapy to elicit synergistic genotoxicity against prostate cancer. *ACS Appl. Mater. Interfaces* **7**, 6661–6673
47. Tartaglia, L. A., Ayres, T. M., Wong, G. H., and Goeddel, D. V. (1993) A novel domain within the 55 kd TNF receptor signals cell death. *Cell* **74**, 845–853
48. Lucas, R., Garcia, I., Donati, Y. R., Hribar, M., Mandriota, S. J., Giroud, C., Buurman, W. A., Fransen, L., Suter, P. M., Nunez, G., Pepper, M. S., and Grau, G. E. (1998) Both TNF receptors are required for direct TNF-mediated cytotoxicity in microvascular endothelial cells. *Eur. J. Immunol.* **28**, 3577–3586
49. Yan, Z., Zhao, N., Wang, Z., Li, B., Bao, C., Shi, J., Han, W., and Zhang, Y. (2006) A mutated human tumor necrosis factor-alpha improves the therapeutic index *in vitro* and *in vivo*. *Cytotherapy* **8**, 415–423
50. Li, M., Qin, X., Xue, X., Zhang, C., Yan, Z., Han, W., Komarck, C., Wang, T. D., and Zhang, Y. (2010) Safety evaluation and pharmacokinetics of a novel human tumor necrosis factor-alpha exhibited a higher antitumor activity and a lower systemic toxicity. *Anticancer Drugs* **21**, 243–251
51. Kuroda, K., Miyata, K., Shikama, H., Kawagoe, T., Nishimura, K., Takeda, K., Sakae, N., and Kato, M. (1995) Novel muteins of human tumor necrosis factor with potent antitumor activity and less lethal toxicity in mice. *Int. J. Cancer* **63**, 152–157
52. Mukai, Y., Shibata, H., Nakamura, T., Yoshioka, Y., Abe, Y., Nomura, T., Taniai, M., Ohta, T., Ikemizu, S., Nakagawa, S., Tsunoda, S., Kamada, H., Yamagata, Y., and Tsutsumi, Y. (2009) Structure-function relationship of tumor necrosis factor (TNF) and its receptor interaction based on 3D structural analysis of a fully active TNFR1-selective TNF mutant. *J. Mol. Biol.* **385**, 1221–1229
53. Nomura, T., Abe, Y., Yoshioka, Y., Nakagawa, S., Tsunoda, S., and Tsutsumi, Y. (2010) [Creation of TNFR1-selective antagonist and its therapeutic effects] [in Japanese]. *Yakugaku Zasshi* **130**, 63–68
54. Nomura, T., Abe, Y., Kamada, H., Inoue, M., Kawara, T., Arita, S., Furuya, T., Minowa, K., Yoshioka, Y., Shibata, H., Kayamuro, H., Yamashita, T., Nagano, K., Yoshikawa, T., Mukai, Y., Nakagawa, S., Tsunoda, S., and Tsutsumi, Y. (2010) Creation of an improved mutant TNF with TNFR1-selectivity and antagonistic activity by phage display technology. *Pharmazie* **65**, 93–96
55. Swanson, T. A., Krueger, S. A., Galoforo, S., Thibodeau, B. J., Martinez, A. A., Wilson, G. D., and Marples, B. (2011) TMPRSS2/ERG fusion gene expression alters chemo- and radio-responsiveness in cell culture models of androgen independent prostate cancer. *Prostate* **71**, 1548–1558
56. Van Bokhoven, A., Varella-Garcia, M., Korch, C., Johannes, W. U., Smith, E. E., Miller, H. L., Nordeen, S. K., Miller, G. J., and Lucia, M. S. (2003) Molecular characterization of human prostate carcinoma cell lines. *Prostate* **57**, 205–225
57. Santo, L., Siu, K. T., and Raje, N. (2015) Targeting cyclin-dependent kinases and cell cycle progression in human cancers. *Semin. Oncol.* **42**, 788–800
58. Van den Heuvel, S., and Harlow, E. (1993) Distinct roles for cyclin-dependent kinases in cell cycle control. *Science* **262**, 2050–2054
59. Orlando, S., Gallastegui, E., Besson, A., Abril, G., Aligué, R., Pujol, M. J., and Bachs, O. (2015) p27Kip1 and p21Cip1 collaborate in the regulation of transcription by recruiting cyclin-Cdk complexes on the promoters of target genes. *Nucleic Acids Res.* **43**, 6860–6873
60. Meulmeester, E., and Jochemsen, A. G. (2008) p53: a guide to apoptosis. *Curr. Cancer Drug Targets* **8**, 87–97
61. Coppe, J. P., Itahana, Y., Moore, D. H., Bennington, J. L., and Desprez, P. Y. (2004) Id-1 and Id-2 proteins as molecular markers for human prostate cancer progression. *Clin. Cancer Res.* **10**, 2044–2051
62. Paolella, B. R., Havrda, M. C., Mantani, A., Wray, C. M., Zhang, Z., and Israel, M. A. (2011) p53 directly represses Id2 to inhibit the proliferation of neural progenitor cells. *Stem Cells* **29**, 1090–1101
63. Chen, G., Gong, R., Shi, X., Yang, D., Zhang, G., Lu, A., Yue, J., and Bian, Z. (2016) Halofuginone and artemisinin synergistically arrest cancer cells at the G1/G0 phase by upregulating p21Cip1 and p27Kip1. *Oncotarget* **7**, 50302–50314
64. Goldar, S., Khaniani, M. S., Derakhshan, S. M., and Baradaran, B. (2015) Molecular mechanisms of apoptosis and roles in cancer development and treatment. *Asian Pac. J. Cancer Prev.* **16**, 2129–2144
65. Fiandalo, M. V., and Kyprianou, N. (2012) Caspase control: protagonists of cancer cell apoptosis. *Exp. Oncol.* **34**, 165–175
66. Creagh, E. M. (2014) Caspase crosstalk: integration of apoptotic and innate immune signalling pathways. *Trends Immunol.* **35**, 631–640

Received for publication March 17, 2018.
Accepted for publication July 30, 2018.